

Uwe Beck
Thomas Fritz
Nadja Gamer
Thomas Wirth

VAMAS
Versailles Project on
Advanced Materials and
Standards
Technical Working
Area (TWA) 2:
Surface Chemical Analysis

242

Forschungsbericht



Materials Research and Testing operates under the guiding-line:

Safety and reliability in chemical and materials technologies

Objectives

The Federal Institute (Bundesanstalt für Materialforschung und -prüfung, BAM) has its responsibility in the interacting fields of Materials – Chemistry – Environment – Safety, in particular:

- statutory functions for technical safety in the public domain, especially relating to dangerous goods and substances
- collaboration in developing legal regulations like on safety standards and threshold values
- consulting on safety aspects of materials technology and chemistry for the Federal Government and industry
- development and supply of reference materials and reference methods, especially for chemical analysis and materials testing
- assistance in developing standards and technical rules for the evaluation of substances materials, structures and processes with reference to damage prevention, life time prediction, protection of the environment and conservation of economical values.

Activities

BAM is engaged in the interdependent and complementary activities:

- research and development
- testing, analysis, approvals
- consultation and information

National and international cooperation

The tasks of BAM for technology, science, economy and society require interdisciplinary cooperation. BAM collaborates closely with technological institutions in Germany and abroad, especially with national institutes. It gives advice to Federal Ministries, economy associations, industrial enterprises and consumer organizations. It provides expertise to administrative authorities and law-courts. In the area of measurement, standardization, testing and quality assurance BAM is the competent national authority for testing techniques. BAM is cooperating with numerous technical, legislative and standardization bodies in order to develop technical rules and safety regulations and represents the Federal Republic of Germany both on the national and international level.

Status

BAM is a senior technical and scientific Federal Institute with responsibility to the Federal Ministry of Economics and Technology. It is the successor of the Public Materials Testing Office (Staatliches Materialprüfungsamt) founded in 1871 and of the Chemical-Technical State Institute (Chemisch-Technische Reichsanstalt) set up in 1920. BAM has a staff of about 1600, including over 700 scientists and engineers working at the main grounds of Berlin-Lichterfelde and at the extensions at Berlin-Steglitz and Berlin-Adlershof.

Uwe Beck
Thomas Fritz
Nadja Gamer
Thomas Wirth



VAMAS

**Versailles Project on Advanced
Materials and Standards
Technical Working Area (TWA) 2:
Surface Chemical Analysis**

**Project A4:
Evaluation of Multilayer Reference
Coatings for Quantitative Glow Discharge
Optical Emission Spectrometry (GD-OES)
and other Depth Profiling Techniques
Report on an Inter-laboratory Comparison**

Forschungsbericht 242

Berlin, Juni 2001

Impressum

Forschungsbericht

Herausgegeben von
Bundesanstalt für Materialforschung und -prüfung (BAM)
Unter den Eichen 87, 12205 Berlin
Telefon (030) 81 04-0
Telefax (030) 8 11 20 29

Copyright © 2001 by Bundesanstalt für Materialforschung und -prüfung

Herstellung und Verlag:
Wirtschaftsverlag NW
Verlag für neue Wissenschaft GmbH
Bürgermeister-Smidt-Str. 74-76, 27511 Bremerhaven
Postfach 10 11 10, 27611 Bremerhaven
Telefon (0471) 9 46 44-0
Telefax (0471) 9 45 44 77/88

D 468

Layout: BAM-G.1

ISSN 0938-5533

ISBN 3-89701-713-X

Contents

1	Introduction	5
2	Project goals	6
3	Sample preparation	6
3.1	Material selection	6
3.1.1	Substrate materials	6
3.1.2	Layer materials	7
3.2	Layer design	7
3.2.1	Ti/Al – multilayers	8
3.2.2	TiO ₂ /SiO ₂ – multilayers	9
4	Sample characterisation	9
4.1	General remarks	9
4.2	X-ray diffraction at grazing incidence (GIXRD)	10
4.3	Spectroscopic ellipsometry (SE)	13
5	Inter-laboratory comparison on depth profiling	15
5.1	General remarks	15
5.2	Technical equipment	16
5.3	Crater profilometry	18
5.3.1	Ti/Al - multilayers on 100Cr6 steel	20
5.3.2	TiO ₂ /SiO ₂ - multilayers on BK7 glass	24
5.4	Analysis of depth profiling data	25
5.4.1	Ti/Al - multilayers on 100Cr6 steel	26
5.4.2	TiO ₂ /SiO ₂ - multilayers on BK7 glass	32
5.4.3	GD-OES depth profiles vs. crater shape	34
5.5	Modelling (GD-OES)	36
5.5.1	Erosion rate	36
5.5.2	Crater propagation	37
5.5.3	Surface area distribution	38
5.5.4	First entrance times	39
5.5.5	Spectral intensities	39
5.5.6	Simulation of depth profiles	40
5.5.7	Deconvolution of depth profiles	42
5.5.8	Calculation of depth profiles	43
6	Discussion	48
7	Summary and conclusions	49
8	Acknowledgements	49
9	References	50
Appendix 1:	List of participants (in alphabetical order)	51
Appendix 2:	Questionnaire of project	52
Appendix 3:	Sample - laboratory - matrix (anonymous)	57
Appendix 4:	Profilometry: crater volume and area	58

1 Introduction

Glow discharge optical emission spectroscopy (GD-OES) was originally developed for the elemental analysis of bulk materials [1]. Several groups introduced this technique to the analysis of coatings, layer stacks and thin films [2]. In the early nineties, it was shown [first for direct current mode (dc-mode)] that even films of some ten, later on of a few, nanometers could be resolved [3, 4, 5]. In the mid nineties, radio-frequency mode (rf-mode) was applied [2, 6, 7], in particular to the analysis of non-conducting films and bulk materials.

In this period of time, an ISO TC 201 working group was founded in order to begin writing standards for all forms of glow discharge spectroscopy (GDS) and to evaluate the capabilities for surface chemical analysis, in particular for depth profiling of layered systems. It was clear from the beginning that this new, however, emerging technique would require some time before being used as a standard tool of depth profiling [8, 9]. The quantification of depth profiles, i.e. the conversion of intensity-time profiles into concentration-depth profiles, had been developed for dc-mode. However, a lack of reference materials was identified. On the contrary, for rf-mode even the quantification procedure itself had not yet been developed. As a consequence, one of the first activities of the ISO working group was the evaluation of the availability of reference materials, i.e. reference coatings [10]. It turned out that none of the available reference materials was appropriate for GD-OES depth profiling for several reasons. Hence, in 1997 a VAMAS TWA 2 proposal on reference coatings for GD-OES depth profiling was made [11]. According to the VAMAS assessment procedure, this proposal was approved with some minor changes in 1998. Based on the revised proposal, the Federal Institute for Materials Research and Testing (BAM) decided to launch an inter-laboratory comparison on the "Evaluation of multilayer reference coatings for quantitative GD-OES depth profiling" under VAMAS TWA 2.

Major input to the project came from Arne Bengtson (SIMR, Sweden) and Mike Winchester (NIST, USA). Furthermore, Volker Hoffmann (IFW Dresden) acted as a major project partner and advisor. Schott Glas Mainz took responsibility of the preparation of non-conducting reference coatings, whereas conducting reference coatings were produced at BAM. In the course of the project, other depth profiling techniques were implemented on request, too. Hence, this report is not exclusively dedicated to GD-OES depth profiling.

2 Project goals

The main objective was the evaluation of two different reference coating systems, one conducting for the assessment of dc-GD-OES and one non-conducting for the evaluation of rf-GD-OES. Furthermore, the performance of various dc- and rf-systems was to be studied and the trueness of analysis had to be verified. Of course, the reference coating systems themselves (material selection, layer design, layer thickness, ...) had to be checked in terms of whether they would be appropriate for the given purpose.

Preliminary versions of such reference systems had been tested by BAM and IFW prior to the VAMAS project in 1998. As a result of these tests and according to the referees' hints, the project goals were identified as follows:

- (I) production of two sets (conducting and non-conducting type) of reference coating systems: BAM and Schott Glas
- (II) non-destructive evaluation of each individual sample (sample fingerprints) by GIXRD (Ti/Al-multilayers) or by SE (TiO₂/SiO₂-multilayers): BAM
- (III) destructive sample analysis, e.g. cross-sectioning, ball-cratering, surface analysis, SEM, TEM for selected samples: BAM
- (IV) GD-OES depth profiling of samples: VAMAS partners (appendix 1)
- (V) profilometry of GD-OES craters: BAM
- (VI) analysis of GD-OES depth profiles: BAM
- (VII) final report and conclusions: BAM

3 Sample preparation

3.1 Material selection

3.1.1 Substrate materials

According to the referees' comments on the proposal, a restriction was made to two classes of materials: non-conducting (type A) and conducting (type B) materials. Further, it was decided to use materials, i.e. also substrate materials, which are of importance for different industrial branches and which may demonstrate the performance of GD-OES for completely different coating/substrate systems. The selections were made as follows:

Type A substrate material:	borosilicate glass BK7 (major application: optics)
Type B substrate material:	100Cr6 steel (major application: engineering)

Both substrate materials contain one major element [Fe ($\approx 96\%$) for 100Cr6-steel, Si ($\approx 70\%$) for BK 7 glass] and one minor element [Cr ($\approx 1,5\%$) for 100Cr6 steel, B ($\approx 6\%$) for BK7 glass]. This circumstance is useful in order to prove the sensitivity of GD-OES depth profiles at the coating/ substrate interface.

3.1.2 Layer materials

Also, a restriction was made to two different classes of layer materials: one conducting (on conducting substrate) and one non-conducting (on non-conducting substrate). Hence, with respect to conductivity two coating/substrate systems were provided:

Type A layer material: $\text{TiO}_2/\text{SiO}_2$ -multilayer (on BK7 glass)

Type B layer material: Ti/Al -multilayer (on 100Cr6 steel)

Again, the selections were made due to further considerations:

Firstly, industrial importance:

- Ti adhesive coating
 - Ti in TiN tribological, decorative, and electronic applications
 - Ti in TiO_2 optical applications
 - Ti in TiC tribological, and decorative applications
- Al conductive coating
 - Al in AlN tribological, high temperature, and electronic applications
 - Al in Al_2O_3 tribological, electronic, and optical applications
- SiO_2 dielectric (low refractive index), diffusion barrier, electronic, and high temperature applications
- TiO_2 dielectric (high refractive index), electronic, and wave guiding applications

Secondly, different sputter rates (S_r):

$$S_r(\text{Ti}) / S_r(\text{Al}) \approx 0,55$$

$$S_r(\text{TiO}_2) / S_r(\text{SiO}_2) \approx 0,23$$

3.2 Layer design

The stack designs and the nominal layer thicknesses are defined as follows (Figs. 1 and 2):

Type A systems: 5 double layers of 100 nm TiO_2 and 100 nm SiO_2

Type B systems: 5 double layers of 50 nm Ti and 250 nm Al

For combined analysis (i.e. users have systems of both dc- and rf-mode available) it seemed to be useful to have at least one element (Ti) in both layer stacks. The use of two different deposition techniques, i.e. ion-assisted reactive electron-beam evaporation (for type A layers) and dc-sputtering (for type B layers) was intended to enable a wider range of application.

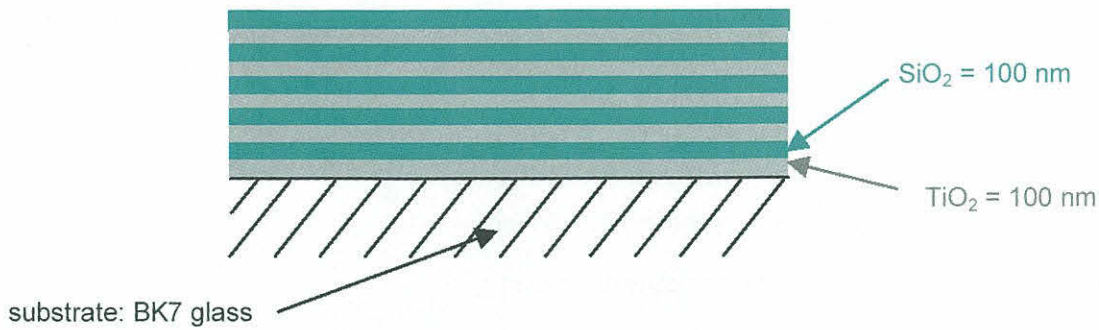


Figure 1: $\text{TiO}_2/\text{SiO}_2$ -multilayer on BK7 glass (type A materials)

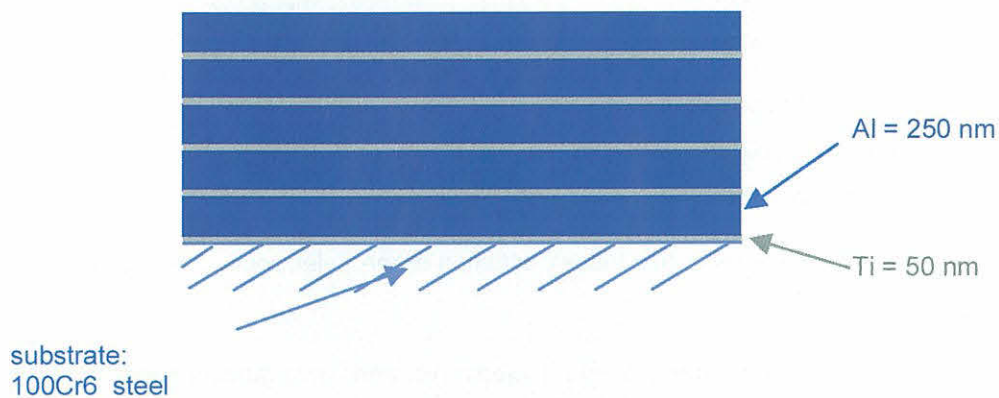


Figure 2: Ti/Al-multilayer on 100Cr6 steel (type B materials)

3.2.1 Ti/Al - multilayers

Inter-laboratory comparison samples of type B (Ti/Al-multilayer on 100Cr6 steel) were produced at the Federal Institute for Materials Research and Testing (BAM), Berlin, Germany. Two sets of samples (batch 158, 30 samples; batch 159, 32 samples) were prepared by means of dc-sputtering in a commercial deposition system HTC 650 from Hauzer Company, the Netherlands.

A post-deposition GIXRD-analysis was carried out for each of the 62 samples (see section 4.2).

According to this analysis, 36 samples were selected for the inter-laboratory comparison. Parameters of the deposition process are given in Table 1. It is a prerequisite to ensure that process temperature is below 180°C . Otherwise, intermetallic phases are generated, and the Ti/Al-multilayer degrades to an intermetallic mixture of titanium and aluminium.

Table 1: Stack design and deposition parameters (batches 158 and 159): Ti/Al-multilayers on 100Cr6 steel

substrate	layer-material	nominal layer thickness h [nm]	layer sequence of deposition	process time t [s]	power $P_{Ti, Al}$ [kW]	Argon flow F [sccm]	temperature T [°C]	dc bias voltage U_{bias} [V]
100Cr6 steel	Ti	50	1,3,5,7,9	200	3	150	170	100
100Cr6 steel	Al	250	2,4,6,8,10	400	4	150	170	100

3.2.2 TiO₂/SiO₂ – multilayers

Inter-laboratory comparison samples of type A (TiO₂/SiO₂-multilayer on BK7 glass) were produced at Schott Glas, Mainz, Germany. Prototypes of type A samples were prepared at the Federal Institute for Materials Research and Testing (BAM) and tested at BAM Berlin and IFW Dresden in order to provide a detailed specification for Schott Glas.

Altogether, 25 samples of type A were sent to inter-laboratory comparison participants. Both TiO₂ and SiO₂ were produced by ion-assisted reactive electron beam evaporation. Process parameters are not presented here as they are subject to proprietary information. The stack design is given in Table 2.

Table 2: Stack design (batch 123591): TiO₂/SiO₂-multilayers on BK7 glass

substrate	layer material	nominal layer thickness h [nm]	layer sequence of deposition
BK7 glass	TiO ₂	100	1, 3, 5, 7, 9
BK7 glass	SiO ₂	100	2, 4, 6, 8, 10

4 Sample characterisation

4.1 General remarks

In addition to non-destructive techniques, i.e. grazing incidence X-ray diffraction (GIXRD, section 4.2) for conducting multilayers of types B and spectroscopic ellipsometry (SE, section 4.3) for non-conducting multilayers of type A, witness samples of type A and B have been destructively analysed by means of several techniques: cross-sectioning, ball grinding, SEM, TEM, and surface analysis. Figs. 3 and 4 show ball grinding craters for both layer types. The accuracy of this technique (with respect to overall layer thickness) is usually not better than $\pm 0,1 \mu\text{m}$ and strongly depends on ball grinding preparation procedure and given materials. In general, the technique is applicable for thicknesses over $1 \mu\text{m}$.

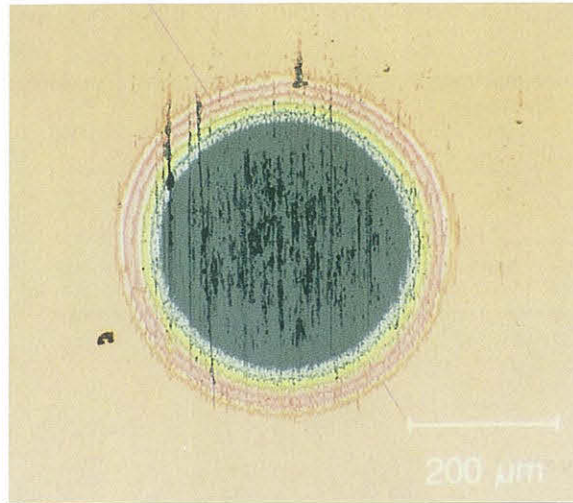


Figure 3: Ball grinding: TiO₂/SiO₂-multilayer on BK7 glass: total layer thickness: $h = (1,1 \pm 0,1) \mu\text{m}$ (batch 123460, sample #95)

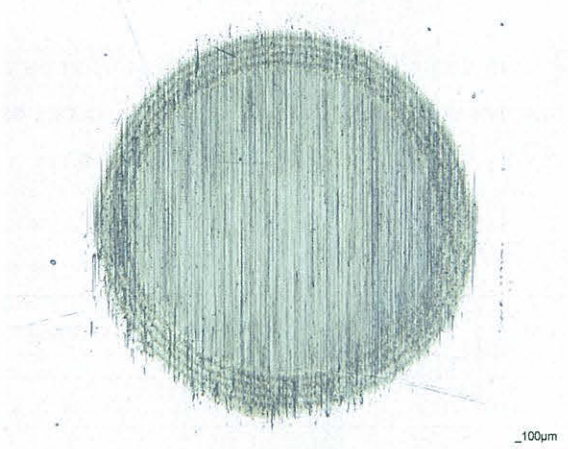


Figure 4: Ball grinding: Ti/Al-multilayer on 100Cr6 steel: total layer thickness: $h = (1,6 \pm 0,1) \mu\text{m}$ (batch 159, sample #345)

Non-destructive techniques of higher accuracy are required for certification. Consequently, each sample was investigated either by GIXRD (type B samples) or by SE (type A samples). As a first estimate, raw data of GIXRD and SE were taken as system fingerprints. Various problems had to be solved with regard to quantification. Crucial points were the texture dependence (GIXRD) and the knowledge of optical constants (SE). With respect to raw data, all inter-laboratory comparison samples were within $\pm 5\%$ from average (GIXRD, type B) and $\pm 1\%$ from average (SE, type A).

4.2 X-ray diffraction at grazing incidence (GIXRD)

GIXRD measurements were taken as non-destructive fingerprints of type B coating/substrate systems. The measurements were performed using a Seifert X-ray diffractometer XRD 3000 TT. Each sample (out of 62 samples) was analysed at an angle of 2° to the surface. The analysing area was 1.5 cm^2 . Hence, X-ray data represented overall information averaged over that area in the centre of the sample.

The objective of the measurements was a classification of the samples according to their X-ray diffraction intensities with reference to the Powder Diffraction File from the International Centre for Diffraction Data. Remarkable differences were observed both for the heights (corresponding to thickness, elemental sensitivity, and crystallinity) of reflex intensities and the ratios of reflex heights (relative texture). Altogether, nine reflexes were considered. Taking the absolute intensity [(peak height in cps) i_{nx} of all reflexes x ($x = 1, \dots, 9$) of all samples P_n ($n = 1, \dots, 30$, respectively 32)], the relative intensity deviation IT_{nx} (normalised intensity, i.e. relative texture deviation from a reference sample) of identical reflexes with respect to the average of this reflex of all samples is calculated as follows:

$$IT_{nx} = \frac{i_{nx} n}{\sum_n i_{nx}} \quad (1)$$

whereas the relative intensity deviation PI_{nx} (sum of all relevant normalised intensities of one sample) with respect to the average of the sums of normalised reflex intensities of all samples is given by:

$$PI_{nx} = \frac{\sum_x IT_{nx} n}{\sum_n \sum_x IT_{nx}} \quad (2)$$

The intensity deviation ΔI (in per cent) of all samples from average, texture-corrected is:

$$\Delta I = 100 (PI_{nx} - 1)$$

Calculated results are given in Tables 3 and 4 whereas a GIXRD diagram of the witness sample batch 158, #433 is shown in Fig. 5. All samples have texture-corrected intensity deviations of less than 5%, except two samples (batch 158, #423 and batch 159, #349). Even for 10% deviation it has been shown by means of SEM analysis of cross-sections that changes of overall thickness are below $\pm 5\%$.

Table 3: GIXRD analysis: batch 158 (30 samples)

sample no.	ΣI_{nx}	PI_{nx}	ΔI [%]
421	9,500	1,054	+ 5,4
423	9,598	1,065	+ 6,5
433	9,173	1,018	+ 1,8
481	8,765	0,973	-2,7
524	9,124	1,013	+ 1,3
531	8,835	0,981	-1,9
532	9,356	1,038	+ 3,8
339	8,756	0,972	-2,8

Table 4: GIXRD analysis: batch 159 (32 samples)

sample no.	ΣI_{nx}	PI_{nx}	ΔI [%]
342	9,104	1,012	-1,2
345	8,636	0,960	+ 4,0
349	8,412	0,935	+ 6,5
352	8,977	0,997	+ 0,3
363	8,746	0,972	+ 2,8
365	9,290	1,032	-3,2
453	9,207	1,023	-2,3
484	8,728	0,970	+ 3,0

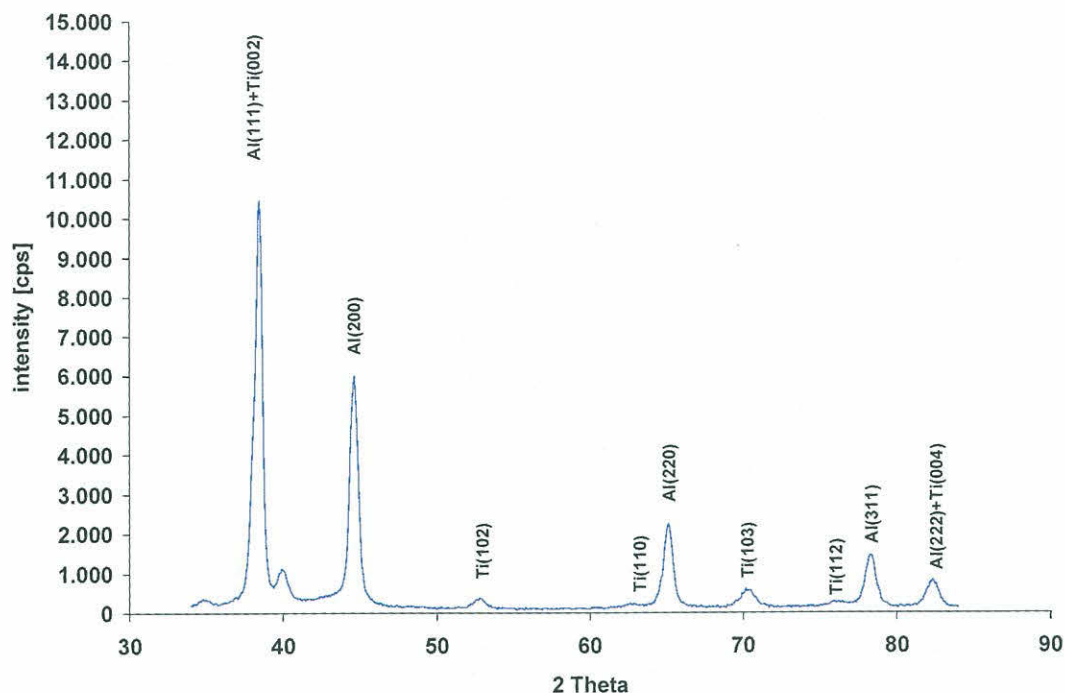


Figure 5: GIXRD-diagram of witness sample # 433, batch 158. All calculated data (Tables 3 and 4) refer to this sample.

4.3 Spectroscopic ellipsometry (SE)

Spectroscopic ellipsometry was used as a fingerprint (raw data Ψ and Δ) technique for each sample of type A. Ellipsometry is a reflection experiment with polarised light. The measurements were performed at three angles of incidence. The typical analysing area was less than 1 mm^2 . For transparent coating/ substrate systems, back side reflection had to be considered. By means of adhesive tape, back side reflection was suppressed for all samples in the same way. Raw data precision was within $\pm 1\%$ for all samples. The same level of uncertainty could have been expected for layer thickness, given that optical constants of bulk and film materials are known. The measurements were performed using a variable angle ellipsometer VASE (J.A. Woollam). Experimental details are given in Table 5.

Table 5: Inter-laboratory comparison samples: experimental details for SE analysis

angle of incidence [°]	wavelength range [nm]	$\Delta\lambda$ [nm]	measurement option	back side reflection
65	270 - 1100	1	without autoretarder	suppressed
70	270 - 1100	1	without autoretarder	suppressed
75	270 - 1100	1	without autoretarder	suppressed

Figs. 6 and 7 demonstrate an ellipsometric spectrum of raw data Ψ and Δ (witness sample #14, batch 123591). As the autoretarder measurement did not provide any additional information, all inter-laboratory comparison samples were measured without autoretarder, i.e. Δ is measured between 0° and 180° .

witness sample #14	(green curve)	(red curve)
wavelength range:	270 nm ... 1700 nm	270 nm ... 1100 nm
wavelength increment:	2,5 nm	1 nm
measurement option:	with autoretarder	without autoretarder
back-side reflection:	suppressed	suppressed

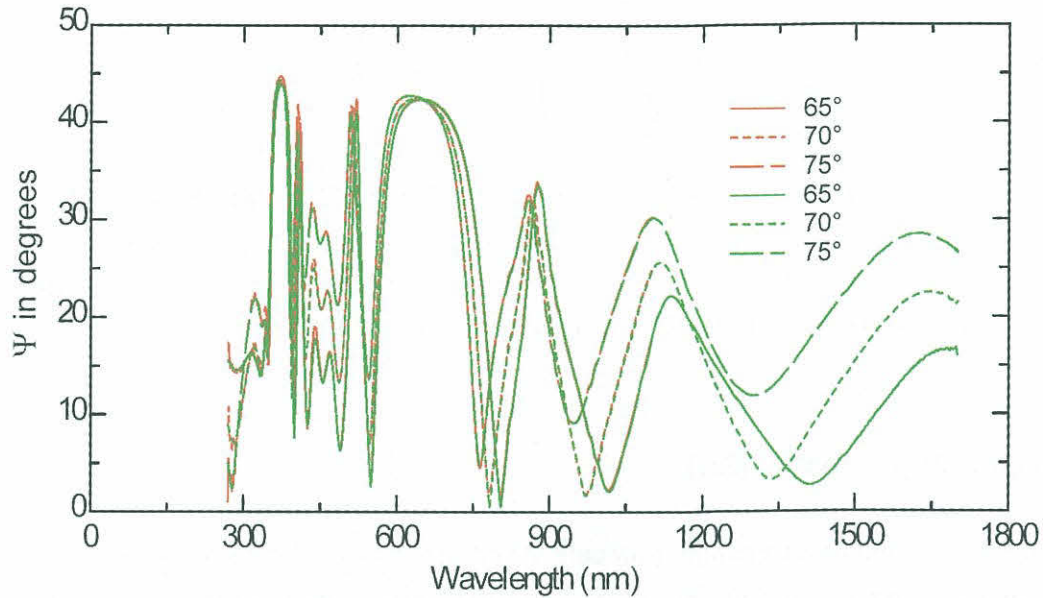


Figure 6: SE-spectrum of witness sample #14 (amplitude information Ψ), batch 123591

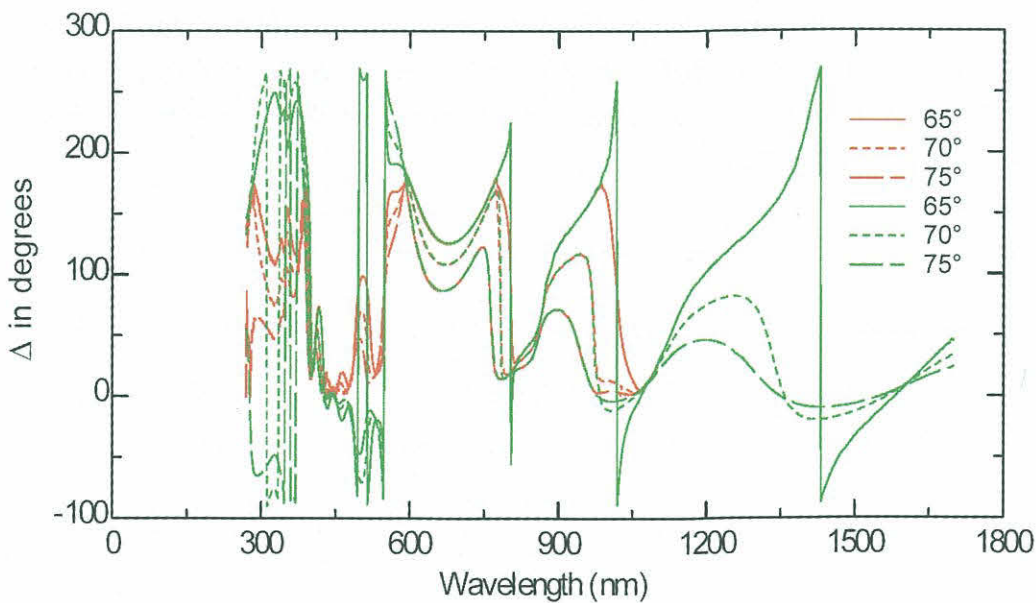


Figure 7: SE-spectrum of witness sample #14 (phase information Δ), batch 123591

5 Inter-laboratory comparison on depth profiling

5.1 General remarks

Two coating/substrate systems were to be evaluated with respect to material selection, layer thickness, layer sequence, sputter rates and their capability to assess depth resolution. These issues were investigated by comparing the results of GD-OES depth profiles of type A and B multilayers taken by inter-comparison partners and using various systems (see appendix 2). The main interest was focused on the ability to resolve the layer structure, the interfaces within the layer stack and between the last layer and the substrate, as well as on the correlation of depth profiles to crater shapes. Based on these results, conclusions have been drawn for an advanced design of such layer stacks [16].

36 laboratories expressed their interest to participate in the inter-laboratory comparison. In the end, 17 laboratories from 10 countries, i.e. Sweden, Finland, France, Slovakia, Austria, Taiwan, USA, Czech Republic, Japan, and Germany, successfully completed depth profiling. They provided results, samples, and additional information as required according to appendix 2 by the end of the year 2000 to BAM for further evaluation. In addition to GD-OES, some other depth profiling techniques were implemented on request. Altogether, results of the following depth profiling techniques have been evaluated: 12x dc-GD-OES, 3x rf-GD-OES, 2x rf-SNMS, 1x dc-GDMS, 1x SIMS (Table 6). Remarkably, just three rf-GD-OES systems succeeded in analysing the completely non-conducting coating/substrate systems of type A.

Table 6: Inter-laboratory comparison participants (laboratory-code), depth profiling techniques, samples received after GD-OES analysis

lab #	dc-GD-OES samples	rf-GD-OES samples	other techniques	Ti/Al on 100Cr6 steel	dc-GD-OES analysis	TiO ₂ / SiO ₂ on BK7-glass	rf-GD-OES analysis
2	x			159-453	yes	-	-
3	x	x		159-484	yes	123591-23	no
11	x			158-532	yes	-	-
12			rf-SNMS	159-342	-	123591-29	-
13	x	x		159-345	yes	123591-30	yes
14			SIMS	158-339	-	-	-
18	x	x		159-352	yes	123591-31	yes
20			dc-GDMS	158-531	-	-	-
21	x	x		158-415	no	123591-19	no
25	x			158-481	yes	-	-
26	x			158-433	yes	-	-
28	x	x		158-524	yes	123591-11	no
29	x			158-468	yes	-	-
30	x	x		159-365	yes	123591-009	no
31	x			159-349	yes	-	-
34			rf-SNMS	158-421	-	123591-005	-
36	x	x		158-423	yes	123591-004	yes

5.2 Technical equipment

All partners had to provide information on the configuration of the analysing system and on technical details of the analysis itself. These data are summarised in Tables 7-9.

Table 7: Experimental set-up of inter-laboratory comparison participants

equipment						system configuration								
sample type	lab #	supplier	poly-chromator	mono-chromator	other	dc-mode	rf - mode		rf/dc - mode			rf-front coupl.	rf-back coupl.	GD-anode diameter d [mm]
							matching type	free running type		matching type	free running type			
B	2	Spectruma	X			X								4
A	3	LECO	X						X			X		4
B	3	LECO	X						X					4
B	11	LECO SDP-750	X			X								4
A	12				SNMS									
A	13	LECO	X						X		X		X	2,5
B	13	LECO	X						X					2,5
B	14	Jobin Yvon		X	SIMS		X						X	4
A	18	Spectruma	X				X							4
B	18	Spectruma	X			X								2,5
B	20	VG 9000			GDMS	X								7
B	25	Spectruma				X								4
B	26	LECO	X			X								4
B	28	lab.-made		X					X			X		8
B	29	LECO	X			X								4
B	30	LECO GDS-750A	X						X	X		X		4
B	31	LECO GDS-750	X			X								4
B	34	Leybold-Heraeus			SNMS				X					3
A	36	LECO	X						X		X		X	2,5
B	36	LECO	X						X		X		X	2,5

Table 8: Analytical parameters (dc-mode operation)

dc-mode *									
		parameter hold constant*				parameter under control*			
sample type	lab #	const. voltage U [V]	const. current I [mA]	const. flow F [sccm]	const. pressure p [Pa]	regulated voltage U [V]	regulated current I [mA]	regulated flow F [sccm]	regulated pressure p [Pa]
B	2	700 / 900					20 / 25		
B	3		19 / 20			700 / 900			
B	11	700						250	50
B	13	700 / 1200						400	
B	18	700 / 1050					10 / 6		X
B	20		0.5		0.009	500			
B	25	700 / 800						850	
B	26	700					20		
B	28	500						530	
B	29		20			700			
B	30		30			800			
B	31	693						410	
B	36	700					20 / 15		

* if two numbers are given in one box, separated by slash (/), left number indicates standard conditions, right number indicates optimised conditions

Table 9: Analytical parameters (rf-mode operation)

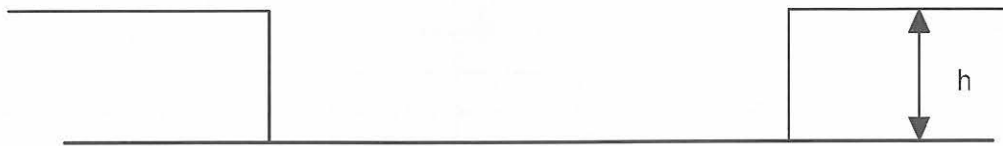
rf-mode												
Sample type	lab #	Ar-flow F [sccm]	Ar pressure p [Pa]	parameter under control								
				a) measured in the rf-generator					b) measured at the sample			
				free running type	matching type							
				U_{pp} [V]	U_{dc} [V]	I_{dc} [mA]	$P_{forward}$ [W]	$P_{reflected}$ [W]	U_{rf} [V]	I_{rf} [mA]	P_{rf} [W]	U_{bias} [V]
A	12	*	*									
A	13	203	500						920	300	3	
B	13	400	770						600	225	15	
B	14	450	400				15	<2				
A	18		400				35	0				
A	34		0,1				170	~35				
A	36	150	70	4200								
B	36	400	50	1400								

* no data received

5.3 Crater profilometry

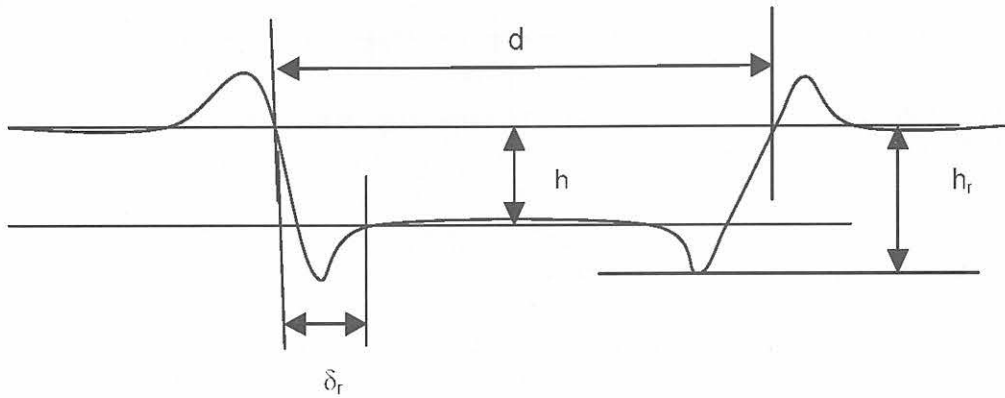
All inter-laboratory comparison samples of type A (3x GD-OES and 1x SNMS) and type B (12x GD-OES, 1x GDMS, 1x SNMS and 1x SIMS) which were sent back to BAM were analysed by profilometry. A mechanical stylus system, Perthometer S6P from Mahr, was used for the classification of craters. As GD-OES craters have been generated under different discharge conditions, two craters per sample have been measured (i.e. one under standard conditions and one under optimised conditions). Fig. 8 shows a schematic classification of crater profiles.

ideal profile



real profiles:

type (i)



type (ii)

(best case)



type (iii)

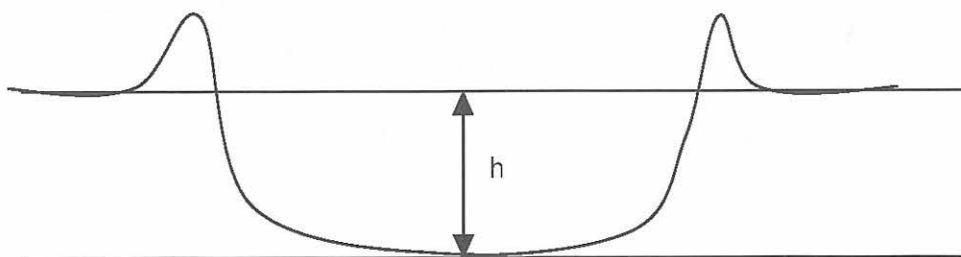


Figure 8: Schematic classification of craters by profilometry

Measured profiles are shown in Figs. 9-11. Quantitative results of measurement are given in Tables 10-11.

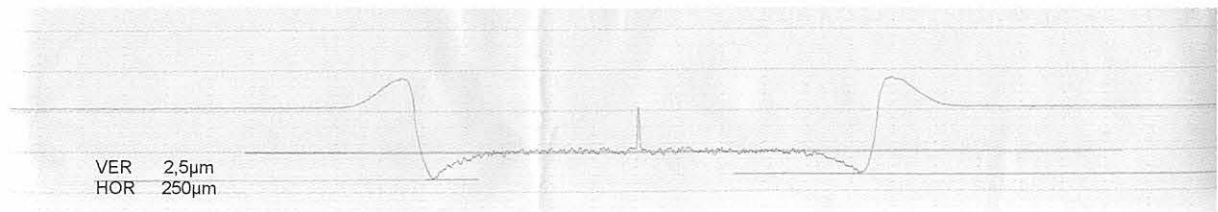


Figure 9: Profile corresponding to crater type (i)

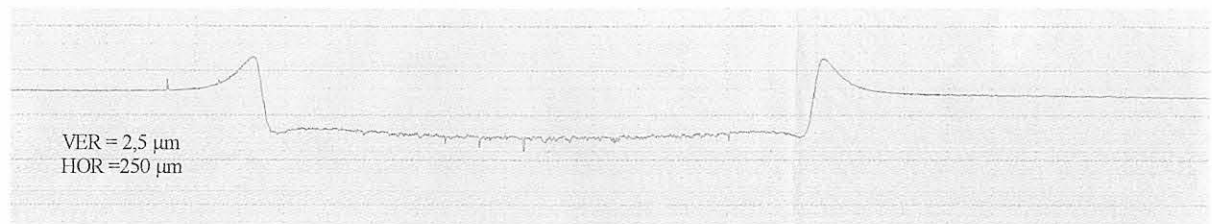


Figure 10: Profile corresponding to crater type (ii)

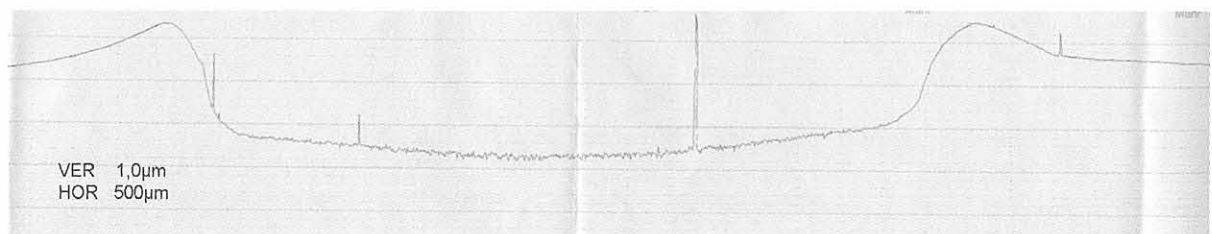


Figure 11: Profile corresponding to crater type (iii)

5.3.1 Ti/Al-multilayers on 100Cr6 steel

Measured quantities were: diameter of crater (d), total depth (mean value) in the centre of the crater (h), maximum depth at the rim of the crater (h_r), and corresponding width (δ_r), see Fig. 8, type (i) and Fig. 12. Volumes and areas of craters were calculated by using these data. The corresponding graphics are presented in Figs. 13-16. The numerical results are given in Tables 24-26 of appendix 4.

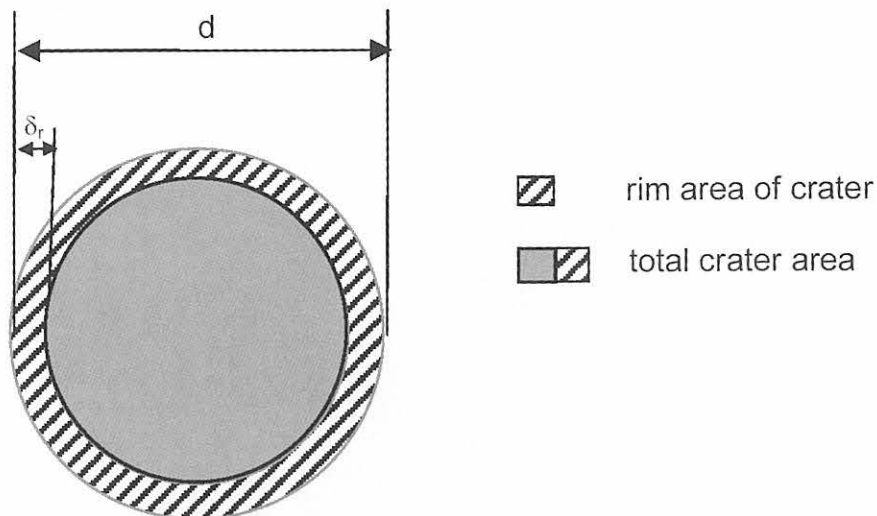


Figure 12: Crater top view, schematic diagram

Table 10: Profilometry: crater cross-section for Ti/Al on 100Cr6 steel (standard conditions)

lab no	crater designation	crater classification	h [μm]	d [mm]	h_r [μm]		$(h_r - h)/h$		δ_r [μm]		δ_r/d	
					left rim	right rim	left rim	right rim	left rim	right rim	left rim	right rim
2	6	i	2,30	4,78	4,75	3,75	1,07	0,63	200	305	0,04	0,06
3	B1	i	3,60	4,80	5,30	5,10	0,47	0,41	231	196	0,05	0,04
13	3 (rf) 4 (dc)	i / i	3,15	2,83	4,30	3,75	0,37	0,19	184	136	0,07	0,05
			3,13	2,80	4,00	3,63	0,28	0,16	195	163	0,07	0,06
18	cc	i	5,50	2,75	9,00	8,50	0,64	0,55	378	345	0,14	0,13
25	2	i	1,63	4,80	2,50	2,88	0,53	0,77	293	363	0,06	0,08
26	B	i	4,50	4,95	5,63	5,63	0,25	0,25	125	150	0,03	0,03
29	3	i	2,38	4,85	3,00	3,13	0,26	0,32	150	175	0,03	0,04
31	10 / 12	i	1,88	4,90	2,88	3,00	0,53	0,60	200	175	0,04	0,04
			1,80	4,83	3,44	2,50	0,91	0,39	172	194	0,04	0,04
36	02	iii	7,50	3,33	-	-	-	-	-	-	-	-

Table 11: Profilometry: crater cross-section for Ti/Al on 100Cr6 steel (optimised conditions)

lab no	crater designation	crater classification	h [μm]	d [mm]	h _r [μm]		(h _r - h)/h		δ_r [μm]		δ_r/d	
					left rim	right rim	left rim	right rim	left rim	right rim	left rim	right rim
2	1	i	2,75	5,00	6,10	4,80	1,22	0,75	422	486	0,08	0,10
3	B5	i	3,80	4,73	6,80	6,00	0,79	0,58	333	294	0,07	0,06
11	1	iii	3,30	4,90	-	-	-	-	-	-	-	-
	3		3,00	4,90	-	-	-	-	-	-	-	-
13	5	i	3,00	2,83	4,00	4,00	0,16	0,16	87,50	75,00	0,03	0,03
14	2 (rf)	iii	12,00	4,95	-	-	-	-	-	-	-	-
18	ea	i	5,05	3,00	6,20	6,05	0,23	0,20	83,00	105	0,03	0,04
20	1	iii	$\approx 1,6$	$\approx 8,7$	-	-	-	-	-	-	-	-
25	6	i	2,40	4,80	4,13	4,50	0,72	0,88	273	337	0,06	0,07
28	1	iii	$\approx 2,2$	$\approx 9,6$	-	-	-	-	-	-	-	-
30	2	i	2,70	4,93	4,30	3,70	0,59	0,37	243	155	0,05	0,03
36	3 (dc)	iii / ii	6,50	3,25	-	-	-	-	-	-	-	-
	16(rf)		2,50	3,15	-	-	-	-	-	-	-	-

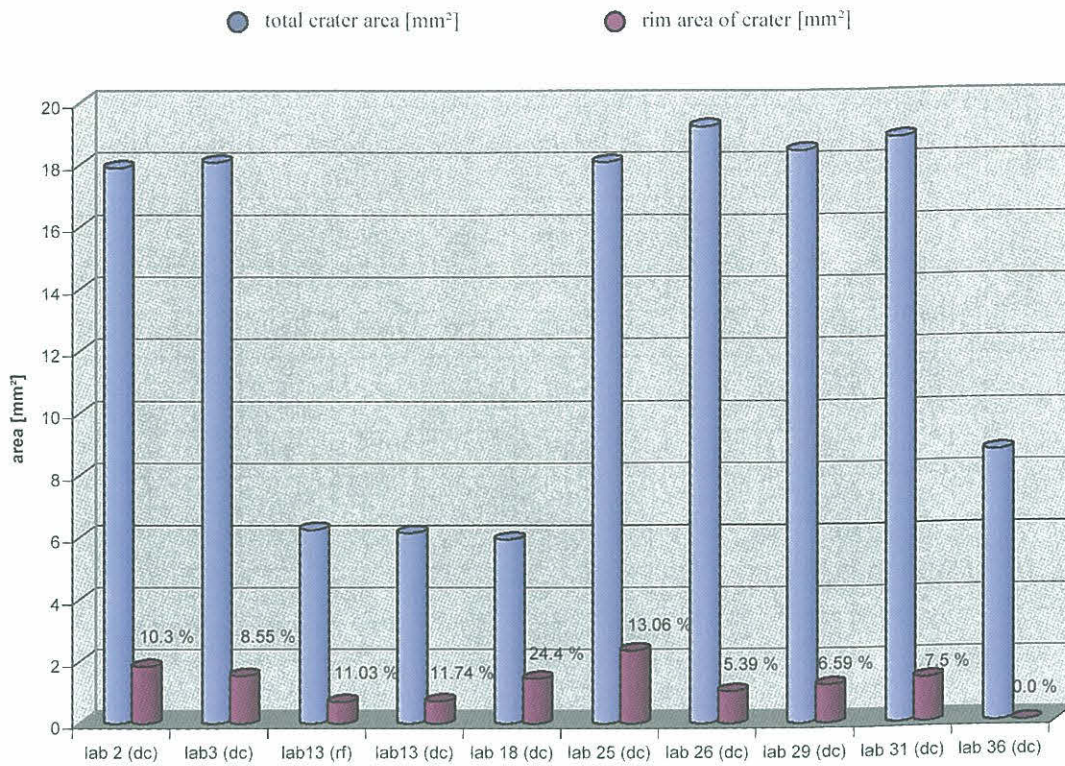


Figure 13: Crater area Ti/Al-multilayer on steel (standard conditions)

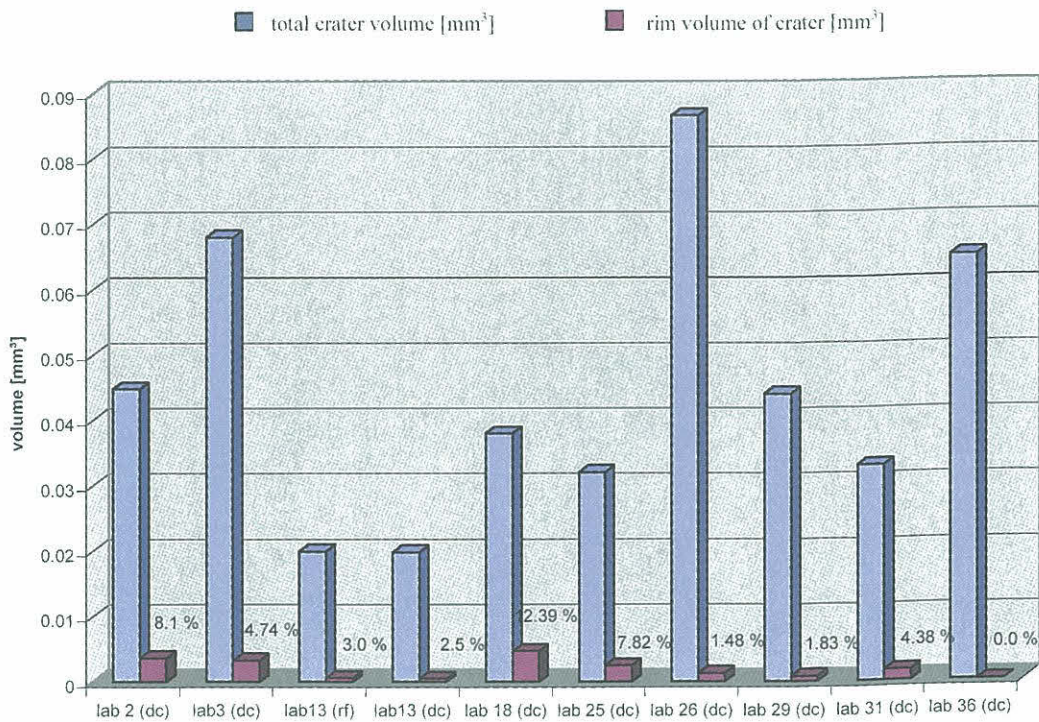


Figure 14: Crater volume Ti/Al-multilayer on steel (standard conditions)

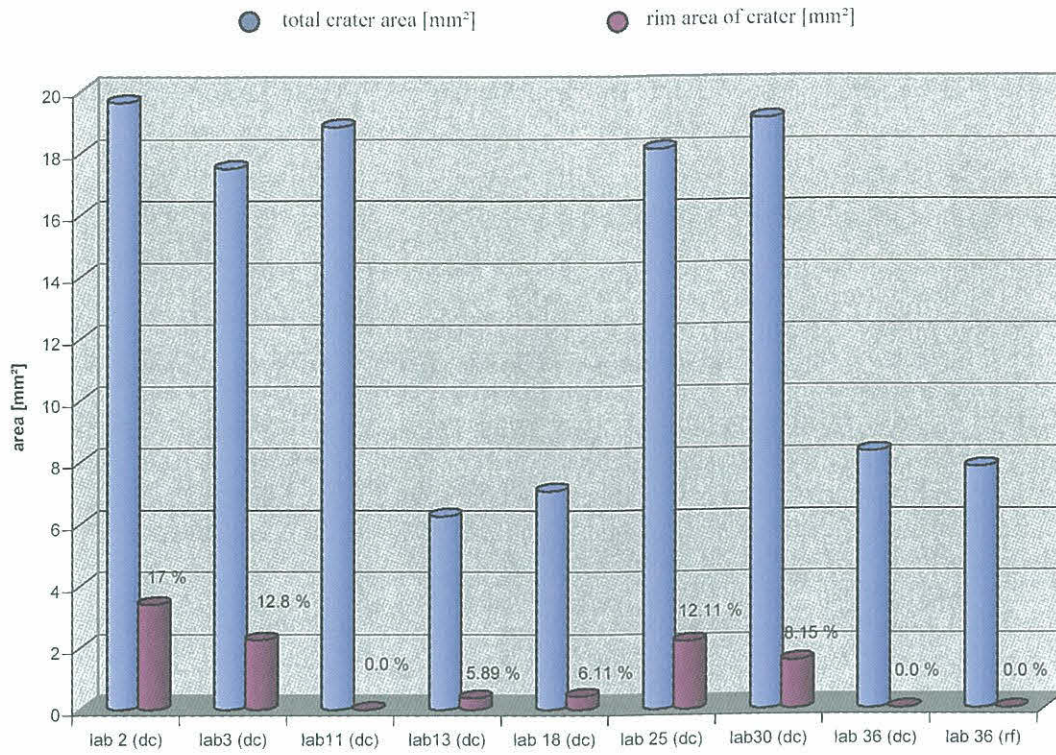


Figure 15: Crater area Ti/Al-multilayer on steel (optimised conditions)

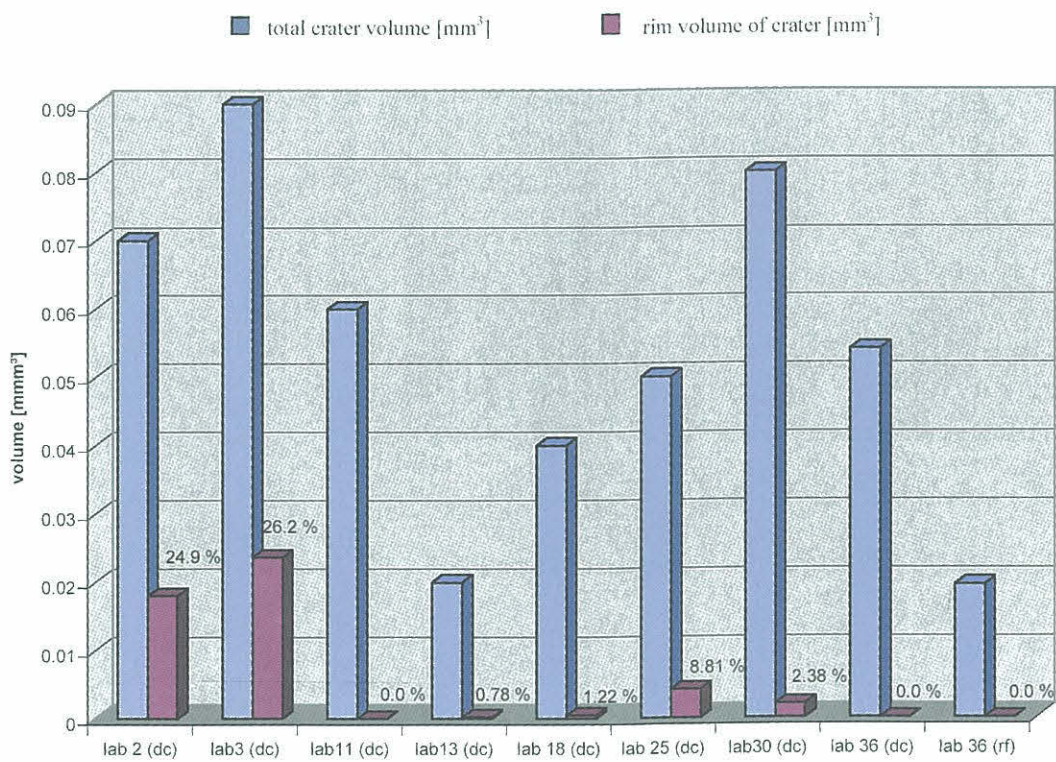


Figure 16: Crater volume Ti/Al-multilayer on steel (optimised conditions)

5.3.2 TiO₂/SiO₂ – multilayers on BK7 glass

The evaluation was made analogous to section 5.3.1. The results are given in Table 12 and Figs. 17-18.

Table12: Profilometry: crater cross-sections of TiO₂/SiO₂ on BK7 glass

lab no	crater designation	crater classification	h [μm]	d [mm]	h _r [μm]		(h _r - h)/h		δ _r [μm]		δ _r /d	
					left rim	right rim	left rim	right rim	left rim	right rim	left rim	right rim
13	1	i	1,50	2,70	2,20	2,30	0,47	0,53	400	500	0,15	0,19
	5		1,31	2,63	1,50	1,50	0,15	0,15	175	150	0,07	0,06
18	2	iii	2,75	3,95								
34	10	ii	2,00	3,78								
36	5	i	2,63	2,68	4,00	3,75	0,52	0,43	537	415	0,21	0,15

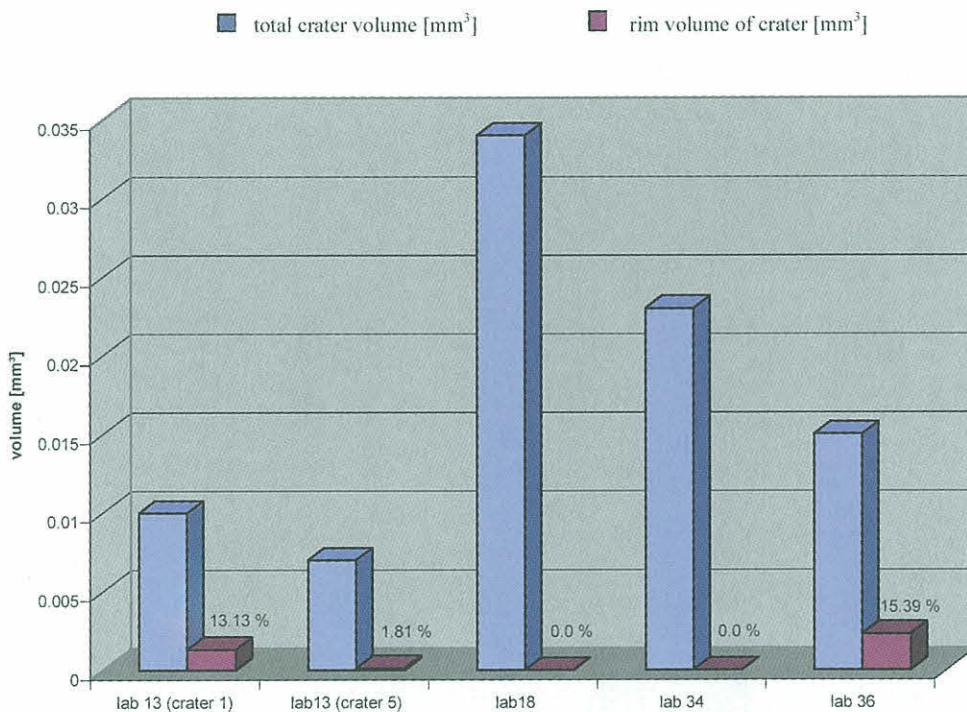


Figure 17: Crater area TiO₂/SiO₂ on BK 7 glass (optimised conditions)

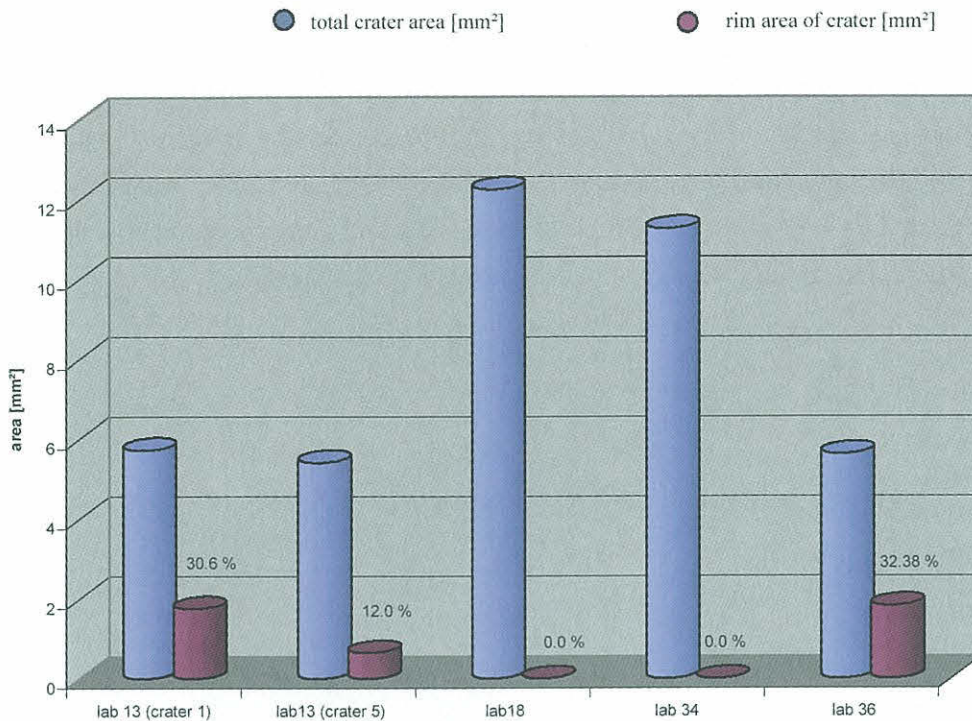


Figure 18: Crater volume of $\text{TiO}_2/\text{SiO}_2$ on BK 7 glass (optimised conditions)

5.4 Analysis of depth profiling data

The relative depth resolution of a layer system is often described by $\Delta z/z$ where Δz is the difference in depth between 84% and 16% of maximum intensity [12]. For depth profiles under evaluation, this rule could not be applied for practical reasons. Another approach is the comparison of sputter times necessary to remove the top (first) layer and the corresponding (last) layer of the same material closest to the substrate. It was clear from the beginning that this was also not feasible because of short sputter times (even for thicker Al layers). Further appropriate values for comparison of depth profiles seemed to be the FWHM's, the slopes of the signal at given positions, as well as the intensity ratios of maximum to minimum. Unfortunately, after checking the FWHM results and the slope data with respect to comparability, an ambiguous behaviour was observed, too. Therefore, the evaluation of layer resolution was performed by comparing maxima/minima ratios „r“ (peak to peak ratios of intensity) for the first (r_f) and the last (r_l) layer interface of selected materials (Al in case of Ti/Al-multilayers, Si in case of $\text{TiO}_2/\text{SiO}_2$ -multilayers). Ideally, the intensity for layer material # 1 (e.g. Al) is zero when layer material # 2 (e.g. Ti) is being analysed. As a consequence, a division by “0” would occur. However, even for ideally rectangular profiles, this case will never occur because of roughness at the crater bottom. By calculating the r_f/r_l ratios, a new parameter $q = r_f/r_l$ was introduced characterising the constancy of layer resolution over depth. This parameter varies between $q = 1$ (r constant over depth) and $q = r_f$ where the last layer cannot be resolved anymore ($r_l = 1$). Additionally, the ratio r_f is related to GDS conditions and crater shape at the beginning of depth profiling given that switch-on effects can be avoided, neglected or eliminated, whereas r_l is more or less related to the same features at the end of analysis.

5.4.1 Ti/Al – multilayers on 100Cr6 steel

For the characterisation of the transition region multilayer/substrate, sputter times at on-set, 10%, 50%, 90%, and 100% of the intensity of Fe signal were used. These different positions are marked in the depth profile shown in Fig. 19. The calculated data for q and $r_f = I_{\max, f} / I_{\min, f}$ (Fig. 19, corrected by switch-on effects) derived from Ti/Al depth profiles are presented in Tables 13 and 14 and Figs. 20 and 21, while Figs. 22-25 and Tables 15 and 16 present Fe intensity data. In Table 17 results derived from measurements by SNMS, SIMS and GD-MS are shown. Fig. 26 provides a comparison of all methods applied.

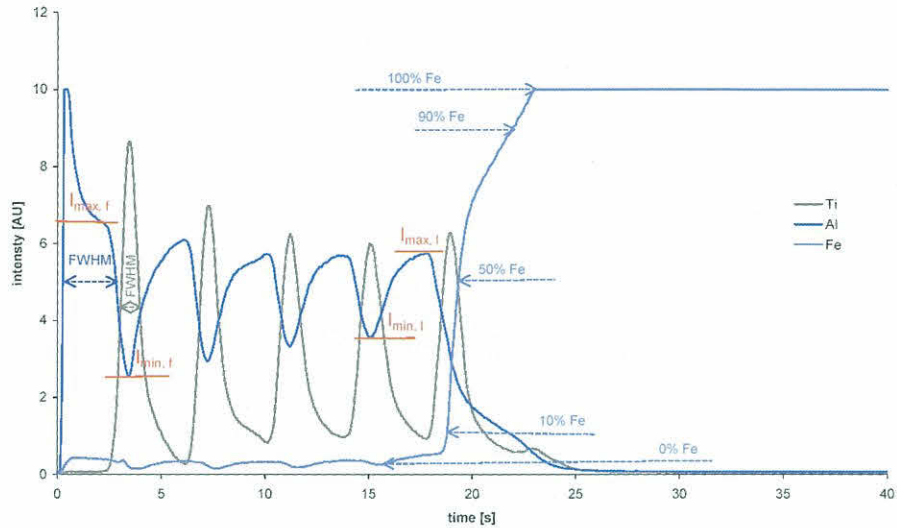


Figure 19: GD-OES-spectrum of Ti/Al on 100Cr6 steel (standard condition, dc-mode; U=700V, I=20mA; lab # 36, batch 158, sample #423)

Table 13: Maximum/minimum Al intensity ratios (r) determined at the first (r_1) and the last (r_f) Al layer of GD-OES depth profiles applying standard conditions

lab #	$q = r_f/r_1$	r_f
2	1,67	2,58
3	1,73	2,64
11	1,87	2,80
13	1,78	2,42
13 (rf)	1,70	2,28
18	1,36	1,98
25	1,92	3,88
26	2,43	4,01
29	2,21	3,28
36	1,62	2,58
average	1,83	-

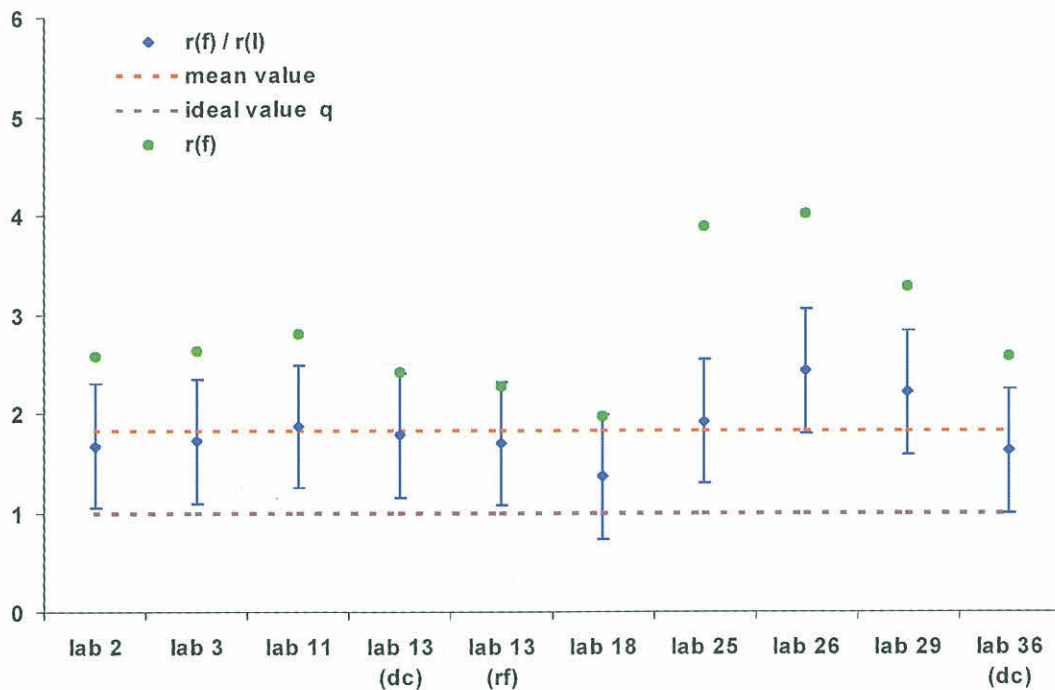


Figure 20: Maximum/minimum Al intensity ratios (r) determined at the first (r_i) and the last (r_f) Al layer under standard conditions

Table 14: Maximum/minimum Al intensity ratios (r) determined at the first (r_i) and the last (r_f) Al layer under optimised conditions

lab #	$q = r_f/r_i$	r_f
2	2,37	2,87
3	1,54	2,43
13	2,18	2,85
18	2,19	2,33
25	1,35	3,19
28	2,17	3,06
30	1,36	2,76
36 (rf)	1,86	2,46
average	1,97	-

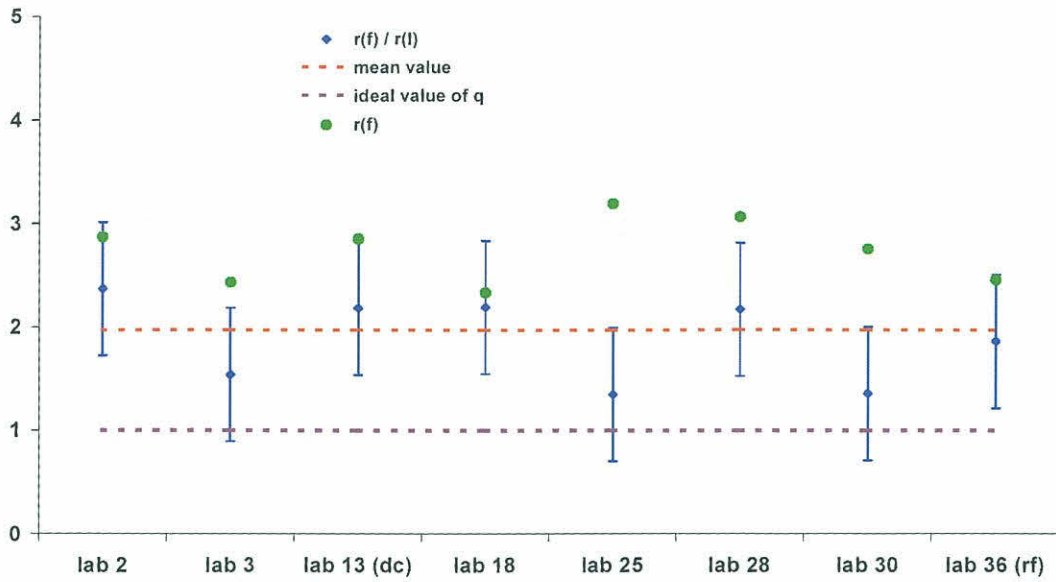


Figure 21: Maximum/minimum Al intensity ratios (r) determined at the first (r_i) and the last (r_f) Al layer under optimised conditions

Table 15: Normalised GD-OES sputter times determined at on-set (0%), 10%, 50%, 90%, and 100% of Fe intensity (standard conditions)

lab #	crater designation	normalised sputter time				
		0%	10%	50%	90%	100%
2	6	0,54	0,64	0,89	0,96	1
3	B1	0,40	0,72	0,85	0,90	1
13	4	0,59	0,60	0,62	0,72	1
18	cc	0,61	0,77	0,90	0,98	1
25	2	0,55	0,67	0,97	0,99	1
26	B	0,53	0,73	0,77	0,90	1
29	3	0,53	0,76	0,87	0,95	1
31	10 / 12	0,59	0,77	0,93	0,96	1
36	02	0,70	0,81	0,83	0,95	1

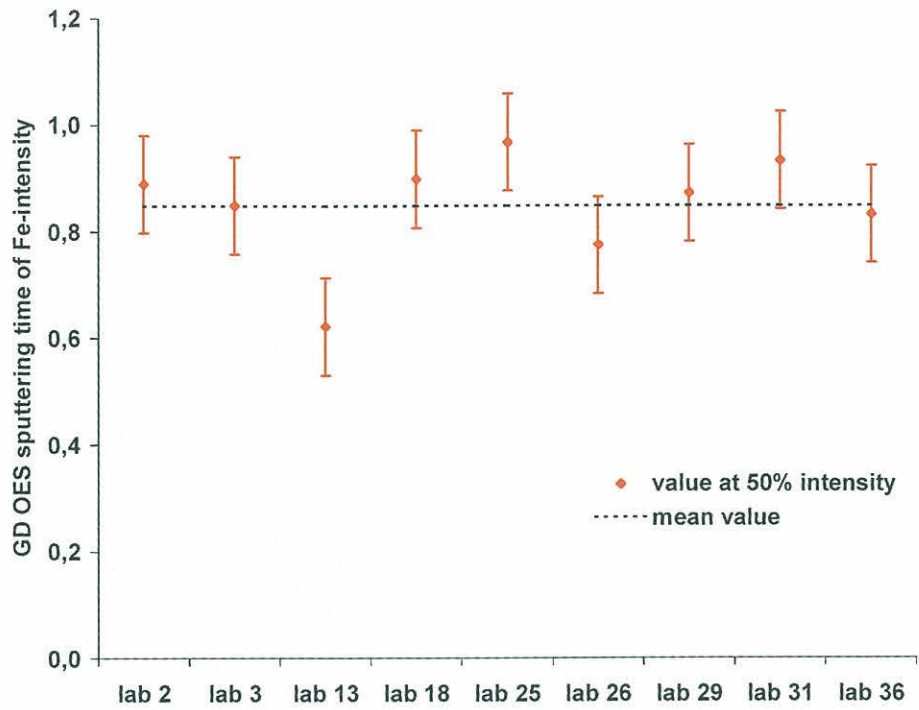


Figure 22: Normalised GD-OES sputter times at 50% of Fe intensity (standard conditions)

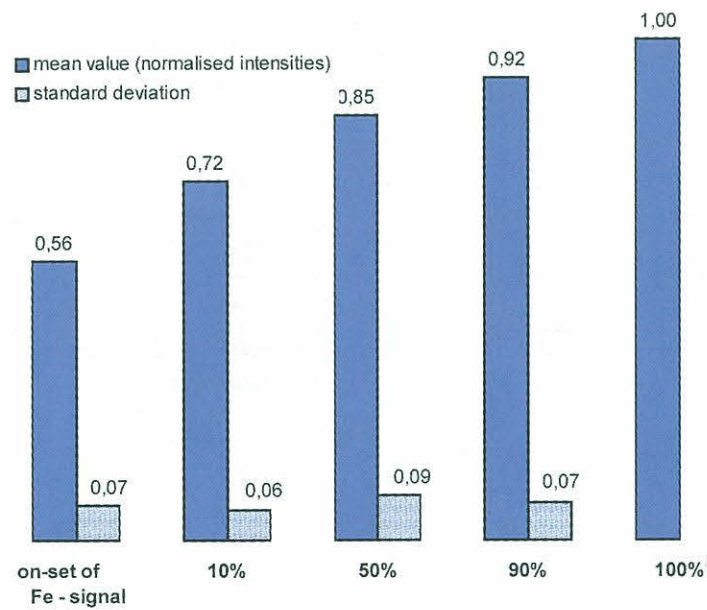


Figure 23: Normalised GD-OES sputter times determined at on-set (0%), 10%, 50%, 90%, and 100% of Fe intensity (standard conditions)

Table 16: Normalised GD-OES sputter times determined at on-set (0%), 10%, 50%, 90%, and 100% of Fe intensity (optimised conditions)

lab #	crater designation	normalised sputter time				
		0%	10%	50%	90%	100%
2	1	0,44	0,64	0,85	0,95	1
3	B5	0,40	0,61	0,88	0,92	1
11	1 / 3	0,76	0,76	0,79	0,95	1
13	5	0,68	0,74	0,84	0,91	1
18	ea	0,49	0,18	0,73	0,91	1
25	6	0,55	0,71	0,93	0,96	1
30	2	0,76	0,88	0,95	0,98	1
36	3 (dc)	0,72	0,72	0,75	0,90	1
36	16(rf)	0,83	0,85	0,87	0,96	1

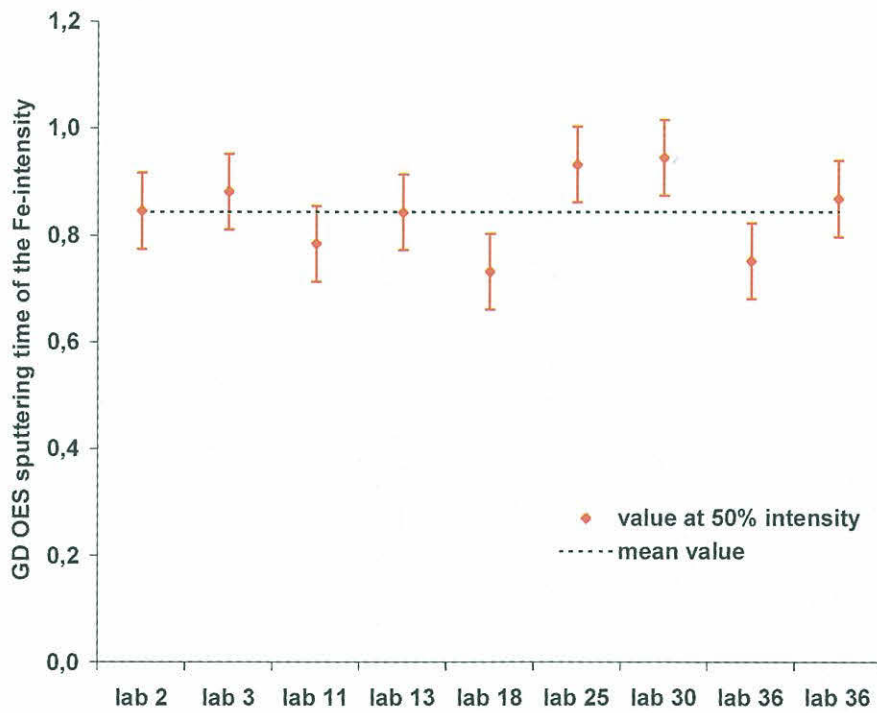


Figure 24: Normalised GD-OES sputter times at 50% of Fe intensity (optimised conditions)

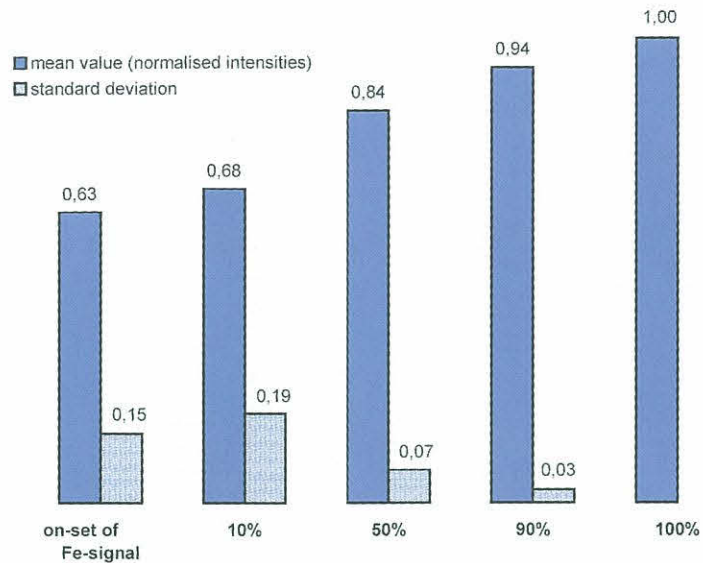


Figure 25: Normalised GD-OES sputter times determined at on-set (0%), 10%, 50%, 90%, and 100% of Fe intensity (optimised conditions)

Table 17: Normalised sputter times determined at on-set (0%), 10%, 50%, 90%, and 100% of Fe intensity for other depth profiling techniques

lab #	techniques	normalised sputter time				
		0%	10%	50%	90%	100%
12	SNMS	0,83	0,87	0,92	0,85	1
14	SIMS	0,92	0,92	0,95	0,98	1
20	GDMS	0,85	0,85	0,87	0,97	1

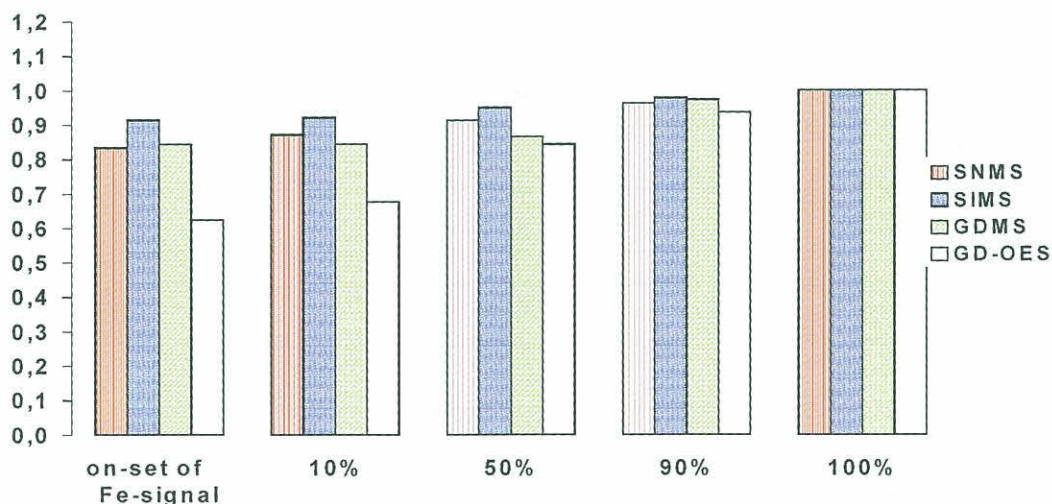


Figure 26: Sputter times determined at on-set (0%), 10%, 50%, 90% and 100% of Fe intensity (optimised conditions): GD-OES and other depth profiling techniques in comparison

5.4.2 TiO₂/SiO₂ – multilayers on BK7-glass

Corresponding data for TiO₂/SiO₂ multilayers are given in Tables 18 and 20 for GD-OES. In Tables 19 and 21 results derived from measurements by SNMS are shown. Figures 28 and 29 present a comparison of both methods applied. Analogous to section 5.4.1, for the characterisation of the transition region multilayer/substrate, sputter times at on-set, 10%, 50%, 90%, and 100% of the B signal were used.

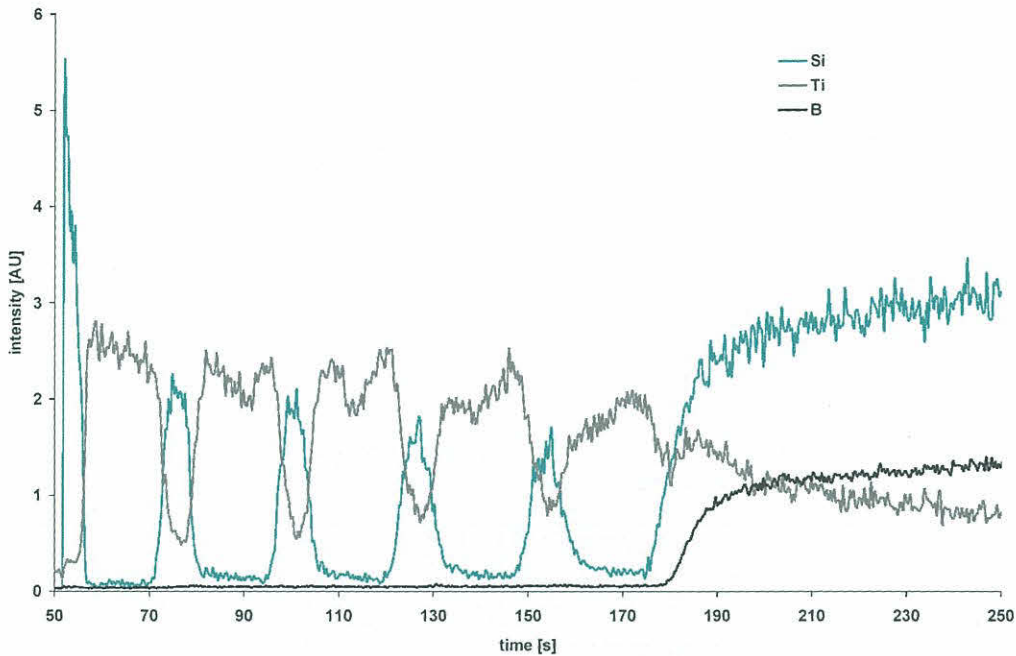


Figure 27: GD-OES-depth profile of TiO₂/SiO₂ on BK7 glass (optimised conditions, rf-mode; U_{RF}=4200V, P=70Pa, F=400 sccm; lab # 13, batch 159, sample # 345)

Table 18: Maximum/minimum Si intensity ratios (r) determined at the first (r_i) and the last (r_f) SiO₂ layer of GD-OES depth profiles applying standard conditions.

lab #	r_f/r_i	r_f
13	1,70	2,02
18	4,08	5,95
36	3,92	3,79
average	3,23	-

Table 19: Maximum/minimum Si intensity (r) ratios determined at the first (r_f) and the last (r_l) SiO_2 layer of SNMS depth profiles.

lab #	r_f/r_l	r_f
12	1,21	20,47
34	1,47	4,62
average	1,34	-

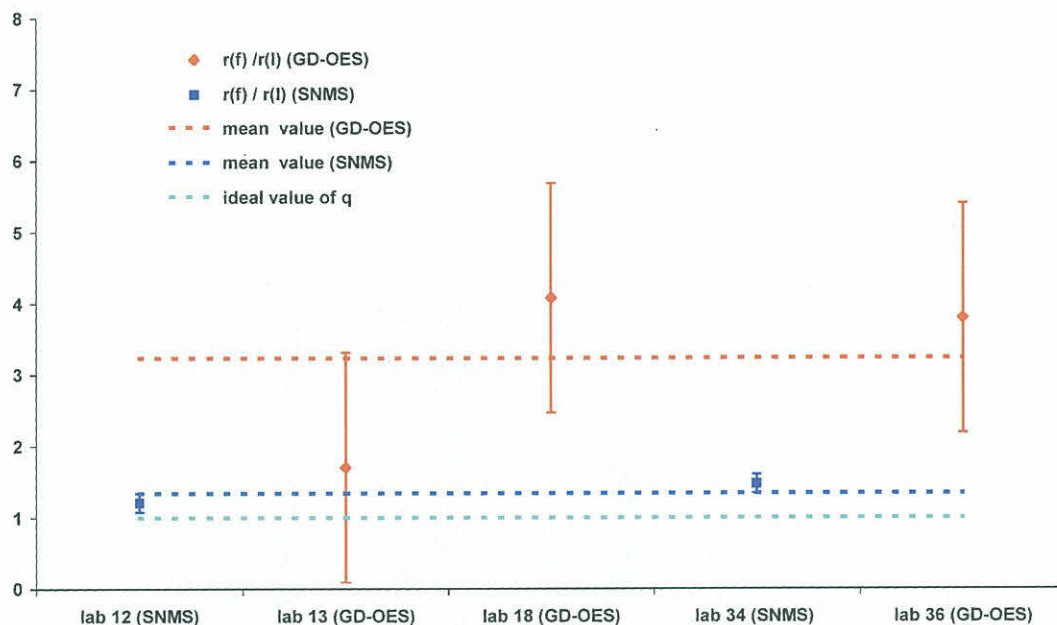


Figure 28: Maximum/minimum Si intensity ratio (r) determined at the first (r_f) and the last (r_l) SiO_2 layer of GD-OES and SNMS depth profiles.

Table 20: Normalised GD-OES sputter times determined at on-set (0%), 10%, 50%, 90%, and 100% of B intensity (optimised conditions)

lab #	crater designation	normalised sputter time				
		0%	10%	50%	90%	100%
13	1	0,87	0,88	0,92	0,97	1*
18	2	-	0,80	0,97	0,97	1
36	5	0,84	0,85	0,95	0,95	1

* 100% intensity of B signal not achieved

Table 21: Normalised SNMS sputter times determined at on-set (0%), 10%, 50%, 90%, and 100% of the B intensity (optimised conditions)

lab #	crater designation	normalised sputtter time				
		0%	10%	50%	90%	100%
12	4	0,92	0,93	0,99	0,99	1
34	10	0,89	0,90	0,91	0,98	1

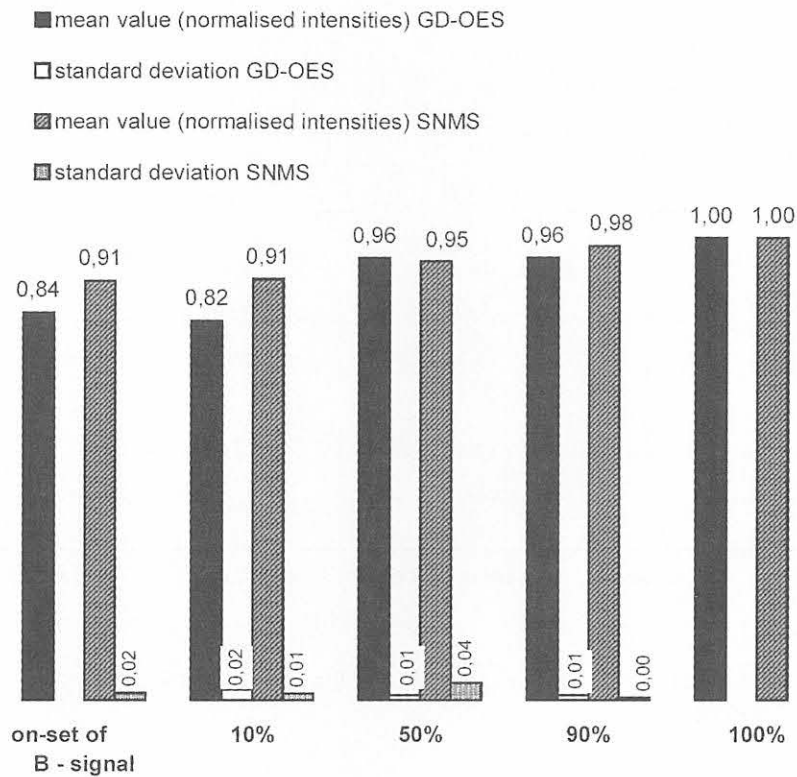


Figure 29: Mean values and standard deviations of GD-OES and SNMS sputter times determined at on-set (0%), 10%, 50%, 90%, and 100% of B intensity (optimised conditions)

5.4.3 GD-OES depth profiles vs. crater shape

The shape of sputter craters at the end of depth profiling should be somehow related to the depth resolution at the coating/substrate interface. Parameters deduced from crater profilometry were compared with results of GD-OES depth profiles. The only correlation that was found concerns the on-set (for convenience the 10% level was used) of Fe signal (respectively B signal). In Tables 22 and 23 data crater rim dimensions are presented together with sputter times at 10% Fe intensity.

Table 22: Depth, mean area, and mean volume of crater rim region as well as sputter times at 10% intensity of Fe signal (standard conditions, Ti/Al-multilayer)

lab #	crater designation	crater classification	(h _r -h)/h		mean rim area [%]	mean rim volume [%]	normalised Fe-intensity to 10%
			left rim	right rim			
2	6	i	1,07	0,63	10,30	8,10	0,64
3	B1	i	0,47	0,41	8,55	4,74	0,72
13	3 (rf)	i	0,37	0,19	11,03	3,01	0,60
	4 (dc)	i	0,28	0,16	11,74	2,50	
18	cc	i	0,64	0,55	24,40	12,39	0,77
25	2	i	0,53	0,77	13,06	7,82	0,67
26	B	i	0,25	0,25	5,39	1,48	0,73
29	3	i	0,26	0,32	6,59	1,83	0,76
31	10	i	0,53	0,60	7,50	4,06	0,77
	12	i	0,91	0,39	7,52	4,70	0,75
36	02	iii	0	0	0,00	0,00	0,81

Table 23: Depth, mean area, and mean volume of crater rims as well as sputter times at 10% intensity of Fe signal (optimised conditions, Ti/Al-multilayer)

lab #	crater designatio	crater classification	(h _r -h)/h		mean rim area [%]	mean rim volume [%]	normalised Fe-intensity to 10 %
			left rim	right rim			
2	1	i	1,22	0,75	17,00	24,90	0,64
3	B5	i	0,79	0,58	12,80	26,20	0,61
11	1 / 3	iii	0,00	0,00	0,00	0,00	0,76
13	5	i	0,16	0,16	5,89	0,78	0,74
18	ea	i	0,23	0,20	6,11	1,22	0,18
30	2	i	0,59	0,37	8,15	2,38	0,88
36	3 (dc)	iii	0,00	0,00	0,00	0,00	0,72
	16(rf)	ii	0,00	0,00	0,00	0,00	0,85

5.5 Modelling (GD-OES)

Comparing the results of depth profiling and crater profiling, correlations between resolution and crater shape are subject to modelling. Based on earlier results [13], a depth profile of a layer stack with ideally smooth interfaces has been calculated, in a first step, assuming a rotationally symmetric crater shape (section 5.5.1). Secondly, depth profiles have been simulated by implementing real crater shapes. The results of both the experimental and the calculated profiles have been compared.

5.5.1 Erosion rate

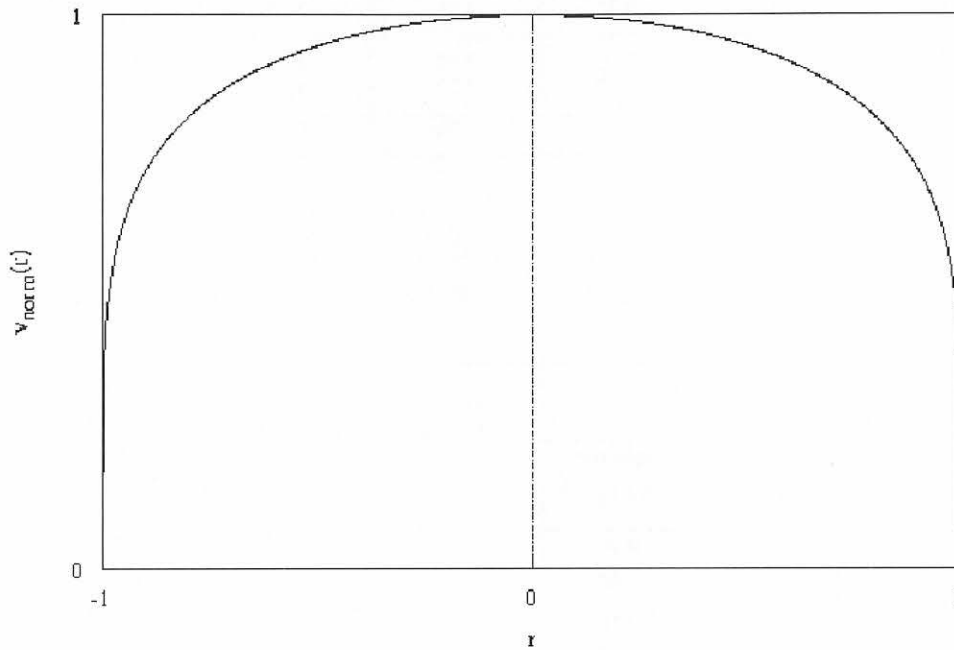


Figure 30: Normalised erosion rate

The crater is assumed to be rotationally symmetric. Any point of the crater is assumed to evolve with its own characteristic velocity (erosion rate) $v(r)$ [4]. Let R be the radius of the crater and v the erosion rate of the medium, i.e. the propagation velocity of the crater at $r = 0$. The normalised erosion rate v_{norm} is defined by

$$v(r) = v \cdot v_{norm}(r/R) \quad (3)$$

In our model we assume v_{norm} to be media independent, depending only on measurement conditions.

Figure 30 shows a normalised velocity profile which may not be very realistic, but it serves as an example here.

$$v_{norm}(r) = (1-r^2)^{1/5} \quad (4)$$

5.5.2 Crater propagation

As discussed in section 5.5.1, crater depth z at time t and radius r is

$$z(t,r) = v \cdot v_{norm}(r/R) \cdot t \tag{5}$$

as long as propagation takes place in one medium. For multilayer media, the situation is more complicated, since sections of the crater surface may propagate in different layers. In general, if the tops of the layers are defined by $z_0 = 0, z_i, i = 1, \dots, n$ and if the erosion rates of the layers are defined by $v_i, i = 1, \dots, n$, and then, if $z(t,r)$ is in the m -th layer, i.e. t is in the time slice

$$\sum_{i=1}^m (z_i - z_{i-1}) / v_i \leq v_{norm}(r) t < \sum_{i=1}^{m+1} (z_i - z_{i-1}) / v_i \tag{6}$$

we have

$$z(t,r) = z_i + v_{i+1} \left[v_{norm}(r) t - \sum_{i=1}^m (z_i - z_{i-1}) / v_i \right] \tag{7}$$

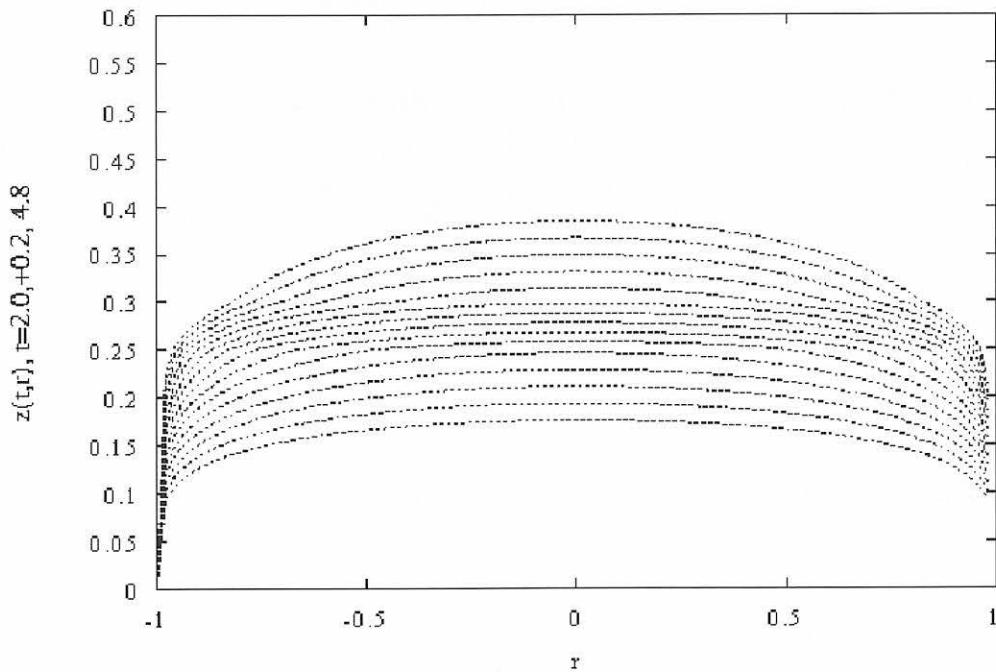


Figure 31: Crater propagation

Figure 31 shows the crater distortions when propagating through a multilayer of 250 nm Al and 50 nm Ti coatings defined by $z_0 = 0.00, z_1 = 0.25, z_2 = 0.30, z_3 = 0.55$ with different erosion rates $v_1 = v_3 = 0.10, v_2 = 0.05$, see also [13, Figure 7].

If we use a depth scale corrected by the erosion rates of the materials, i.e. stretched by the v_i factors, then the depth scale is proportional to the time scale, and the distortions disappear [14, p.864]. This observation is the key for all the calculations: Imagine the time scale as a corrected depth scale, where the crater propagates, i.e. stretches, into the specimen with constant velocity, independent of the material.

5.5.3 Surface area distribution

Since sputtering occurs at the crater surface, we must know how the crater surface area is distributed.

Consider the normalised crater $R = 1$, $v = 1$ at time $t = 1$. Its cross section is (see equation 5)

$$z_{norm}(r) = v_{norm}(r) \quad (8)$$

The surface area element is

$$a(r)dr = 2\pi|r|\sqrt{dr^2 + dz^2} \quad (9)$$

We may omit the term dz because $z_n \ll R$, so that the (lateral) surface element is distributed with density

$$a(r)dr = 2\pi|rdr| \quad (10)$$

along the normalised crater profile. To calculate the total surface density a as a function of z , we have to sum up all surface elements for a given z

$$a(z) = 2\pi \sum_{r \in z_{norm}^{-1}[z]} \left| r \left(\frac{dz}{dr} \right)^{-1} \right| \quad (11)$$

In our example (see equation 4) we have two values $r = \pm\sqrt{1 - z^5}$ for each z , so that

$$\left(\frac{dz}{dr} \right)^{-1} = \frac{dr}{dz} = \frac{-5z^4}{2\sqrt{1 - z^5}} \quad (12)$$

and thus

$$a(z) = 2\pi\sqrt{1 - z^5} \frac{5z^4}{2\sqrt{1 - z^5}} = 5\pi z^4 \quad (13)$$

The corresponding distribution function is

$$A(z) = \begin{cases} 0 & \text{if } z < 0 \\ \int_0^z a(z)dz = \pi z^5 & \text{if } 0 \leq z < 1 \\ \pi & \text{if } z \geq 1 \end{cases} \quad (14)$$

Figure 32 shows a plot of $A(z)$ for the example profile.

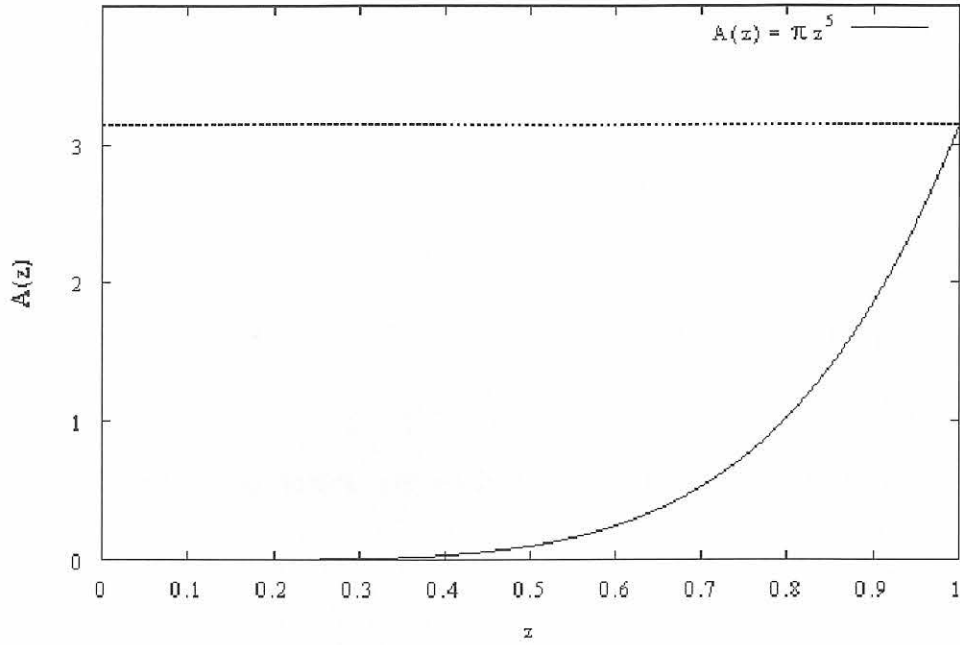


Figure 32: Surface area distribution function

5.5.4 First entrance times

Let $t_0 = 0$, and t_i , $i = 1, \dots, n$ denote the times, when the crater tip is at z_i respectively, i.e.

$$z(t_i, 0) = z_i, i = 0, \dots, n \quad (15)$$

Using Equ. 6 we get

$$t_i = \sum_{j=i}^n (z_j - z_{j-1}) / v_j, i = 1, \dots, n \quad (16)$$

5.5.5 Spectral intensities

The intensity is proportional to the sputter rate, i.e. the eroded volume per time unit. This equals the (lateral) crater surface times the erosion rate. Other authors define the sputter rate as the number of eroded atoms per time unit.

By analogy with Equ. 11 we get

$$q(z) = 2\pi \sum_{r \in z_{norm}^{-1}[z]} \left| r v_{norm}(r) \left(\frac{dz}{dr} \right)^{-1} \right| \quad (17)$$

Using $v_{norm}(r) = z$ and equation 11

$$q(z) = 5\pi z^5 \quad (18)$$

which corresponds to the distribution function

$$q(z) = \begin{cases} 0 & \text{if } z < 0 \\ \int_0^z a(z) dz = \frac{5}{6}\pi^6 & \text{if } 0 \leq z < 1 \\ 1 & \text{if } z \geq 1 \end{cases} \quad (19)$$

The intensity due to layer i at time t is proportional to

$$Q_i(t) = (Q(t_i/t) - Q(t_{i-1}/t))R^2 \quad (20)$$

If the material's concentrations $c(t)$ are distributed continuously rather than sharply defined by a layered structure, then we arrive at

$$Q(t) = \int_0^t c(s)q(s/t)R ds \quad (21)$$

which is, not surprisingly, in accordance with [14].

If we know the emission yield S_i and excitation function E_i , the intensity may be calculated by

$$I_i(t) = E_i S_i Q_i(t) \quad (22)$$

[5, Equ. 3].

5.5.6 Simulation of depth profiles

As an example, consider for Ti /Al-multilayers of alternating coatings of 50 nm Ti, $v = 0.05$, and 250 nm Al, $v = 0.1$, altogether 10 layers on an Fe substrate. This extends the situation of Figure 31. Simulation is carried out without any experimental data. Simulated intensities for each layer material are shown in Figs. 33 and 34. The cumulative intensities are presented in Figure 35. The sputter rate calculated by equation 20 and normalised to one is used as an arbitrary unit for intensities.

VAMAS, Simulation, 5 x (50nm Ti / 250nm Al) on (100Cr₂) steel

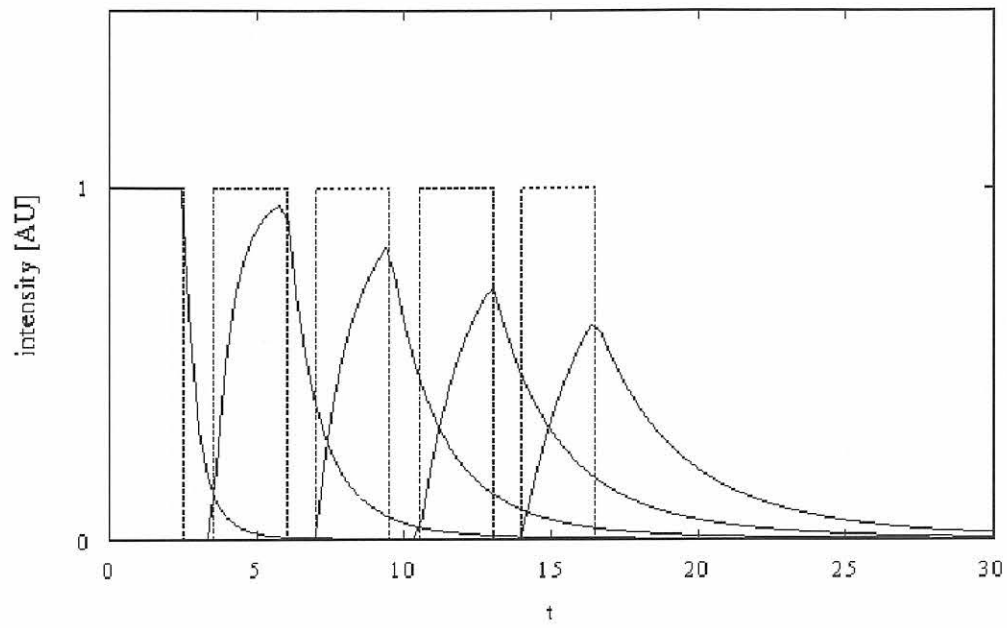


Figure 33: Simulated intensity profile for Al layers

VAMAS, Simulation, 5 x (50nm Ti / 250nm Al) on (100Cr₂) steel

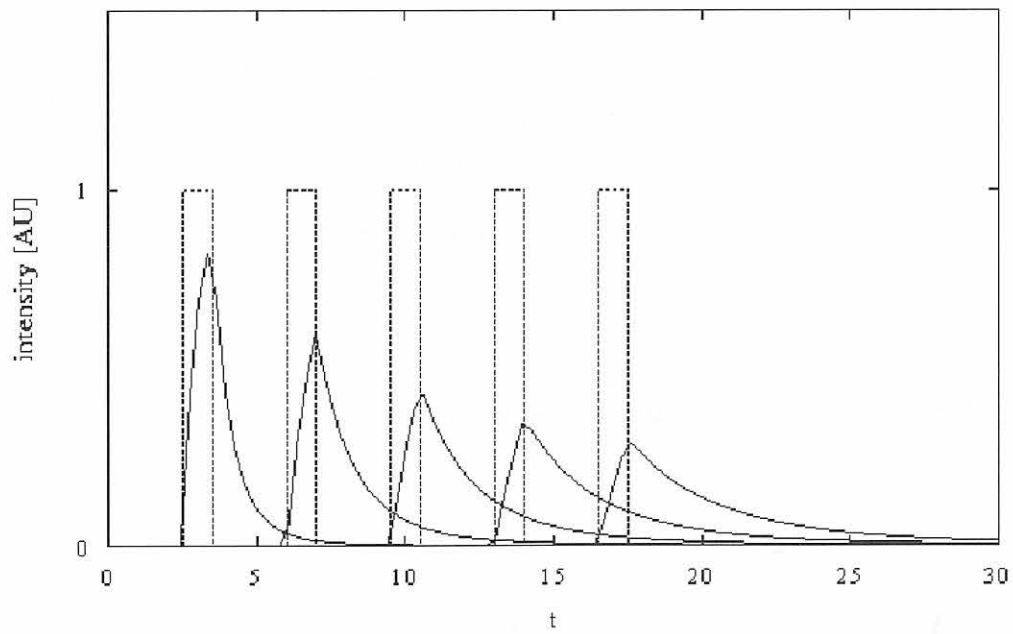


Figure 34: Simulated intensity profile for Ti layers

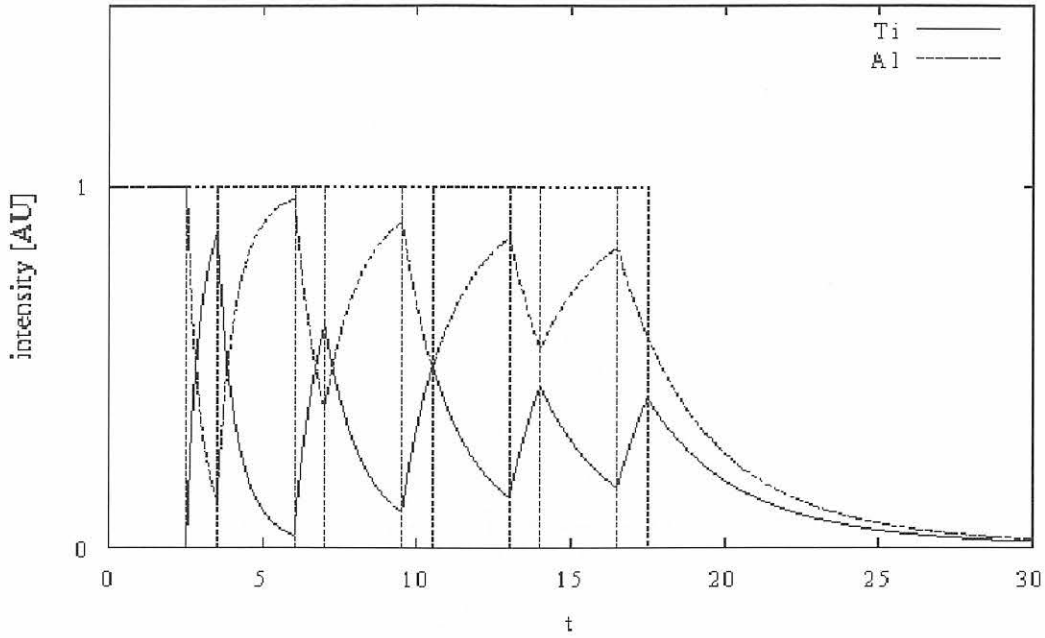


Figure 35: Simulated cumulative intensities for Ti and Al layers

5.5.7 Deconvolution of depth profiles

To calibrate measurement equipment, it is necessary to calculate the sputter rate $Q(t)$ from experimental intensity diagrams of reference materials. For non-layered reference materials, integral equation 21 must be solved numerically. For layered materials the procedure can be simplified.

Assume a single layer and consider equation 20. Since intensity is proportional to the sputter rate inside a layer, one may start with

$$I(t) = Q(t_1/t) - Q(t_0/t) \quad (23)$$

We assume that t_0 and t_1 , i.e. the times when the crater tip enters (exits) the layer, are known from the intensity diagram. Rewrite the last equation for $Q(t_0/t)$ (24)

$$\begin{aligned} Q(t_0/t) &= Q(t_1/t) - I(t) \\ &= 1 - I(t), \quad t \leq t_1 \end{aligned} \quad (25)$$

Substituting t_0/t by t'

$$Q(t') = 1 - I\left(\frac{t_0}{t'}\right), \quad t' \geq \frac{t_0}{t_1} \quad (26)$$

we can calculate $Q(t)$ for times $t \geq t_0/t_1$. The next iteration step gives

$$Q(t') = 1 - I\left(\frac{t_0}{t'}\right) - I\left(\frac{t_0^2}{t't_1}\right), \quad t' \geq \left(\frac{t_0}{t_1}\right)^2 \quad (27)$$

For consistency of these equations note that

$$I\left(\frac{t_0^2}{t't_1}\right) = 0, \quad t' \geq \frac{t_0}{t_1} \quad (28)$$

By multiple iterations, $Q(t)$ can be calculated for all $t > 0$. This is analogous to the Neumann series solving the general integral equation 21. The procedure can be extended to multilayers by summation of equation 20 over all layers of identical material.

5.5.8 Calculation of depth profiles

Using the developed equations, analytical GD-OES depth profiles corresponding to crater types (i), (ii) or (iii) as well as analytical SNMS depth profiles were calculated on the basis of measured profilometry data of the crater (at the end of analysis). The results are shown in Figs. 36 - 39 in comparison to measured depth profiles and crater cross sections.

Lab 36, batch 158, sample #423, crater #2 (standard conditions)

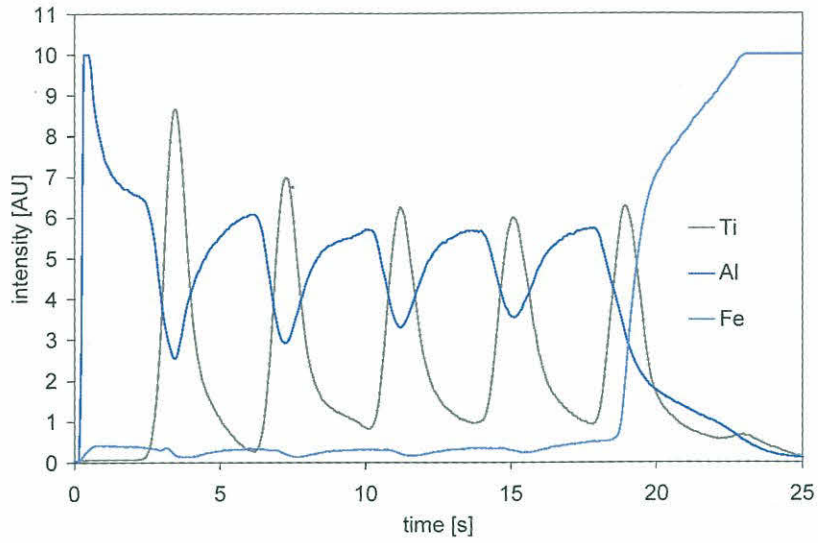


Figure 36 a: dc-GD-OES spectrum of Ti/Al-multilayer on steel

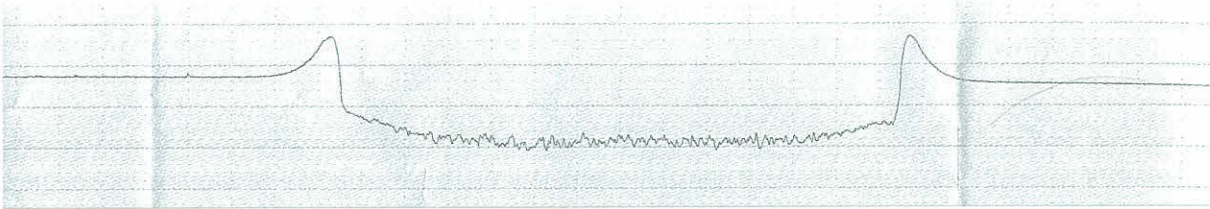


Figure 36 b: Crater profile of Ti/Al-multilayer on steel

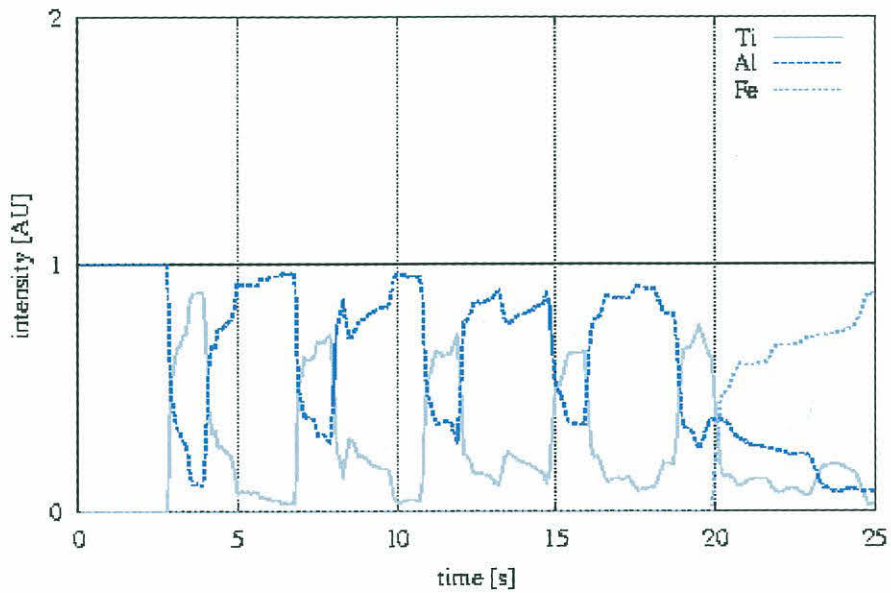


Figure 36 c: Calculated intensity-time profile of Ti/Al-multilayer on steel

Lab 36, batch 158, sample #423, crater #16 (optimised conditions)

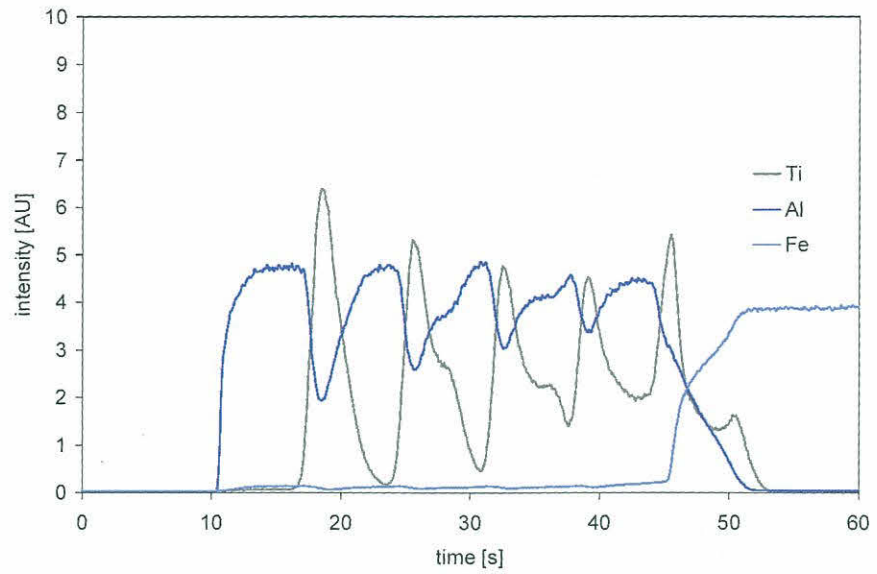


Figure 37 a: rf-GD-OES spectrum of Ti/Al-multilayer on steel

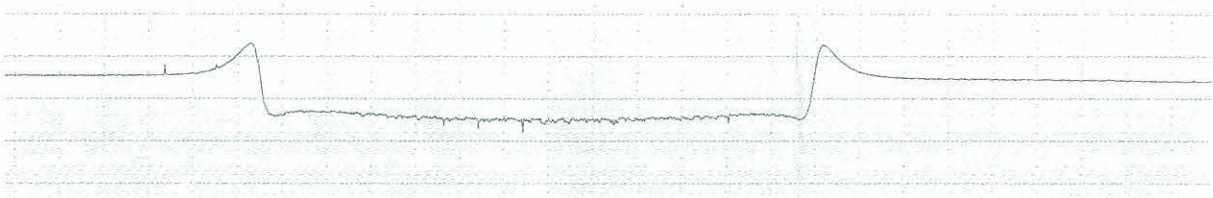


Figure 37 b: Crater profile of Ti/Al-multilayer on steel

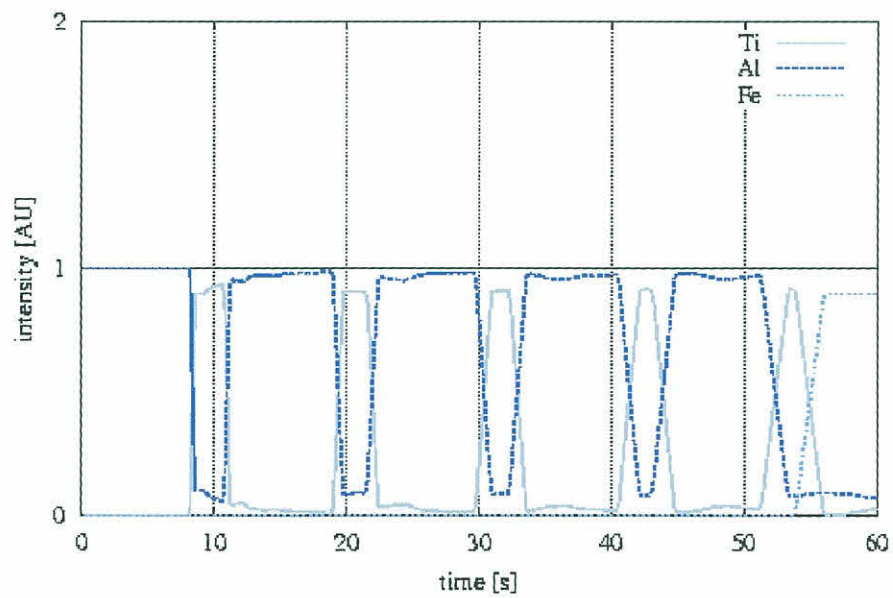


Figure 37 c: Calculated intensity-time profile of Ti/Al-multilayer on steel

Lab 18, batch 159, sample #352, crater #cc (standard conditions)

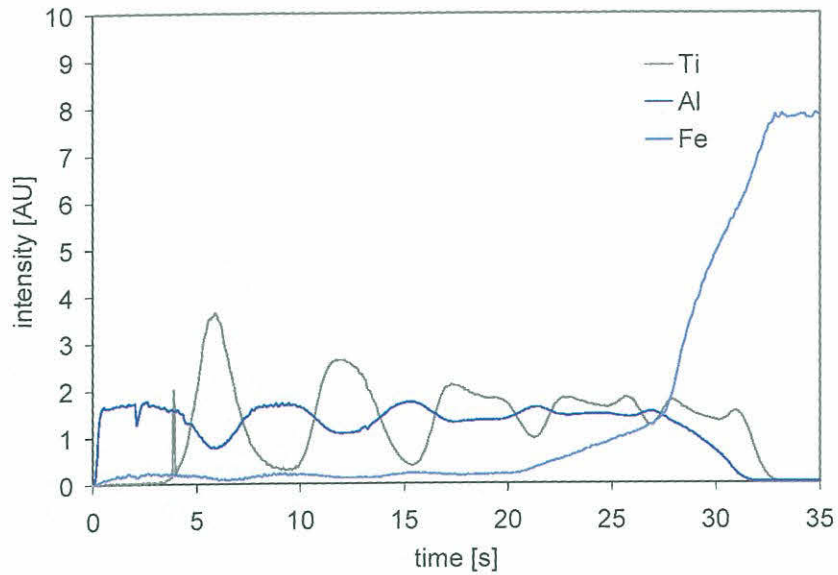


Figure 38 a: dc-GD-OES spectrum of Ti/Al-multilayer on steel

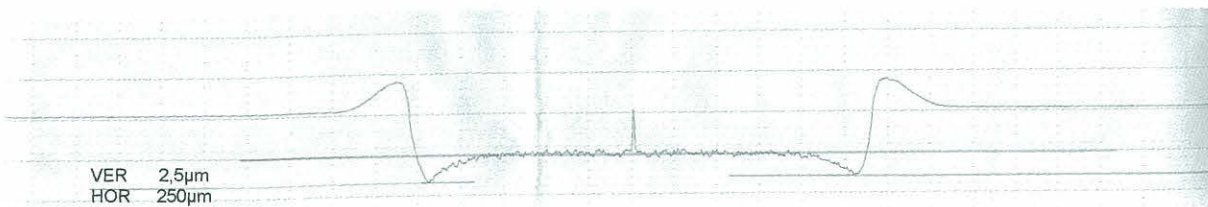


Figure 38 b: Crater profile of Ti/Al-multilayer on steel

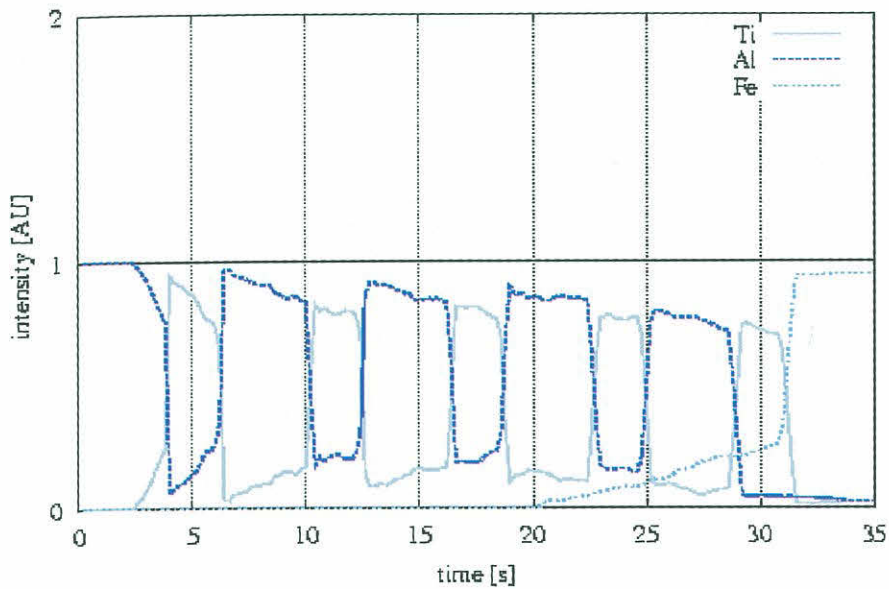


Figure 38 c: Calculated intensity-time profile of Ti/Al-multilayer

Lab 34, batch 123591, sample #005 (optimised conditions)

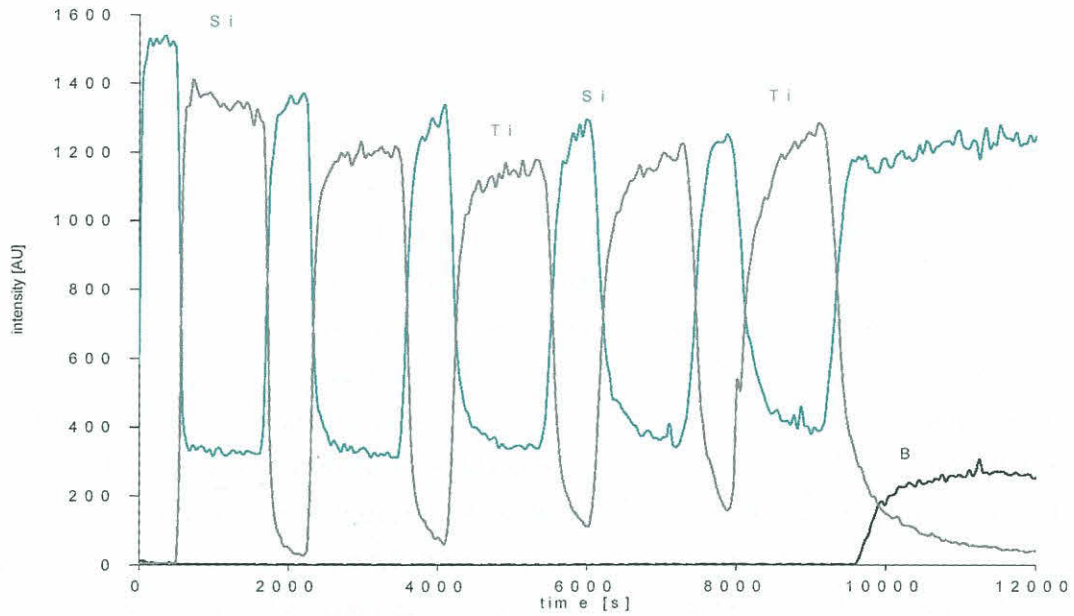


Figure 39 a: SNMS spectrum of $\text{TiO}_2/\text{SiO}_2$ -multilayer on BK7 glass

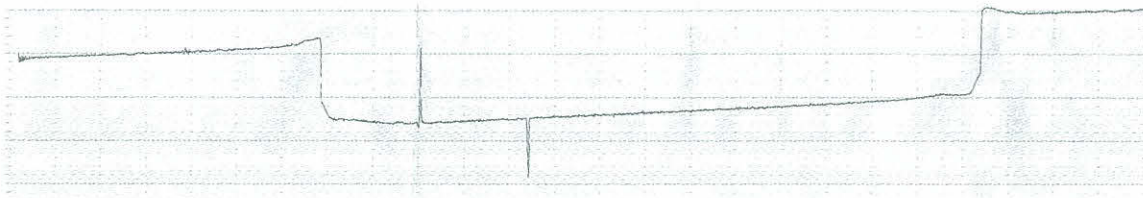


Figure 39 b: Crater profile of $\text{TiO}_2/\text{SiO}_2$ -multilayer on BK7 glass

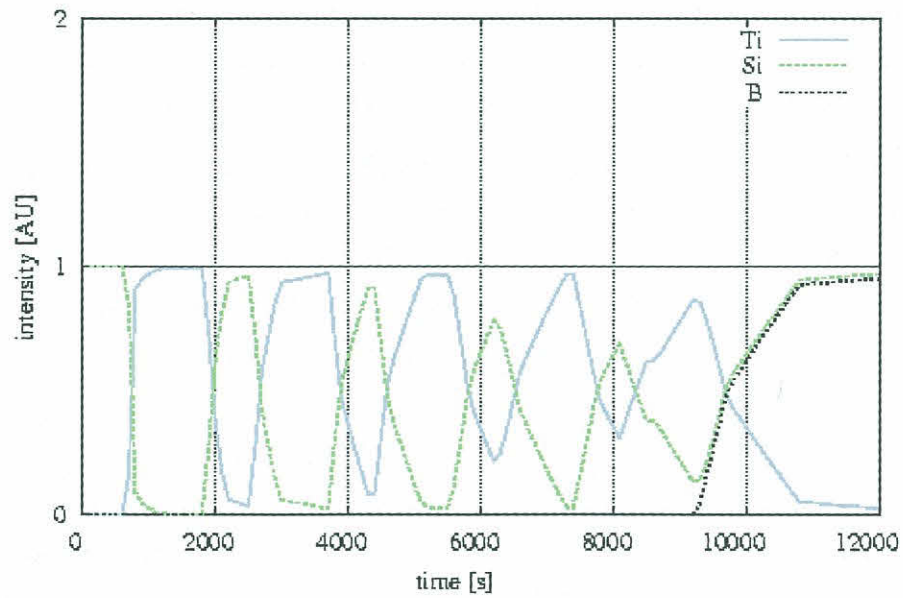


Figure 39 c: Calculated intensity-time profile of $\text{TiO}_2/\text{SiO}_2$ -multilayer on BK7 glass

6 Discussion

Comparing r values of the “first” and the “last” Al layer, not surprisingly, a decrease is found. Discussing the results collected in tables 13 and 14, 18 and 19, ratios r_f and r_l , and hence $q = r_f / r_l$ describe the ability of analysis to resolve the layer structure. For GD-OES, this decrease is caused by crater shape changes and increasing roughness [typically $R_a = (100\text{--}300)$ nm] at the crater bottom. However, in the case of roughness, this statement is valid for other depth profiling techniques as well. Given that switch-on effects can be avoided (i.e. stable discharge from the beginning), suppressed or eliminated, r_f describes the quality of resolution at the first Al layer. The higher the r_f value (after elimination of switch-on effects, see Fig. 19), the better the resolution at the beginning of the depth profile, i.e. crater shape- and roughness-related effects are not pronounced. Analogously, r_l describes the resolution at the last Al layer of the layer stack. Thus, the parameter $q = r_f / r_l$ describes analytically the constancy of layer resolution $\Delta h/h$ over depth and is experimentally related to the features of the GD-OES system and to the quality of the parameter settings of analysis. For $q = 1$, the layer resolution is constant over depth, i.e. “as good” or “as poor” as at the beginning of the analysis. However, under the current circumstances, this has been the only opportunity to compare results of different systems under different discharge conditions and even for different depth profiling techniques. Qualified GD-OES profiles [dc-mode (e.g. Figs. 19, 36a) and rf-mode (e.g. Fig. 27)] demonstrate that r_f (and r_l) can achieve large values roughly constant over depth and thus values of q close to one. One major result is the fact that the crater shape and/or roughness may dramatically change during analysis. As a result, quality of resolution may change (usually gets worse, but sometimes even gets better, e.g. in the case of discharge conditions that are not opt....at the beginning) over sputter depth. This statement is valid for standard and especially not optimised conditions for both dc- and rf-mode. In general, the layer systems themselves, i. e. Ti/Al-multilayers and TiO₂/SiO₂-multilayers, seem to be appropriate for the evaluation of depth profiling. The situation is still different in the case of the substrate materials. Most of the rf-GD-OES systems failed in the analysis of type A coating/substrate systems because of the high impedance of the substrate (1 mm thick glass). As there are many applications on non-conducting substrate materials, e.g. glass and ceramics, this “remaining” technical problem has to be solved in any case.

Poorer depth resolution at the coating/substrate interface (effects of crater shape and roughness on the crater bottom at the end of analysis) usually corresponds to an increasing crater rim and an early on-set of the signal of the substrate material (Fe-signal or B-signal). For some depth profiles, the on-set of the Fe-signal is already found half way into the layer stack. The intensity of the characteristic substrate line grows slowly followed by a steep increase after the complete removal of the last layer.

In the case of depth profiles and crater shapes of SNMS measurements, well resolved layer sequences are found corresponding to craters with low rim areas such as crater type (ii). This is mainly a result of a special source arrangement and lower erosion rates. In contrast, looking at the rf-GD-OES depth profile shown in figure 37, the crater shape is also of crater type (ii) although the resolution of the layer sequence is rather poor. In addition, comparing crater shapes of standard and optimised conditions (Figs. 13-16) two labs provided poorer crater shapes under optimised conditions rather than standard conditions.

On the one hand, comparing experimental depth profiles with analytical depth profiles that had been calculated on the basis of measured crater profilometry data, the calculated profiles show the same

behaviour of decreasing layer resolution with increasing sputter time as the experimental ones do. On the other hand, the profile shape can differ extremely in detail, see in Figs. 37a and c.

From these results, one can conclude that a crater may actually change classification [i.e. type (i), type (ii) or type (iii)] during measurement. Other effects such as plasma instabilities or temperature-, roughness- and material-related effects at the crater bottom and over the entire crater front have to be considered, too.

7 Summary and conclusions

Finally, the conclusion can be drawn that the layer systems under investigation are appropriate for the evaluation of depth resolution $\Delta z/z$ in terms of layer resolution $\Delta h/h$ and for checking GDS conditions. As shown, the selected coating/substrate systems may be useful for other depth profiling techniques as well. The layer materials themselves have been analysed without any problem. As requested by several inter-laboratory comparison participants, the stack design will be slightly modified for Ti/Al multilayers to larger thickness values for Ti layers (increase by a factor of two) in order to get a better first estimate of sputter rates. In general, well characterised layered samples are suitable for checking parameter settings and the GDS conditions, to compare rf- and dc-mode measurements, to determine sputter rates and emission yields, and to evaluate depth resolution. Therefore, the development of layered reference materials consisting of other material combinations is recommended as well.

Regarding rf-analysis, just three out of seven labs successfully performed depth profiles of type A samples. This is clear evidence that rf-GD-OES has not yet become a method for routine analysis as dc-GD-OES has. This was confirmed by the results of the "Expert meeting on radio frequency powered glow discharge sources" of the EC-Thematic Network on Analytical GDS [15]. However, in the present case, the crucial point was the impedance of the non-conducting substrate. Many rf-systems were unable to ignite and to stabilise the discharge for 1 mm thick borosilicate glass. As non-conducting coatings on non-conducting substrates are of great industrial importance, this problem must be overcome. This is a prerequisite for rf-GD-OES to compete with other depth profiling techniques as dc-GD-OES already does.

Based on the results of this VAMAS inter-laboratory comparison and because of the expressions of interest for such coating systems, BAM will provide slightly modified reference coating systems on a commercial basis starting in the year 2002. Details are given in the BAM reference material catalogue [16].

8 Acknowledgements

The authors gratefully acknowledge the co-operation and the advice of A. Bengtson (SIMR, Stockholm), V. Hoffmann (IFW, Dresden), M. Winchester (NIST, Gaithersburg), R. Hentschel, U. Brauneck, R. Mollenhauer (Schott, Mainz).

9 References

- [1] W. Grimm
Spectrochim. Acta 23B, 443 (1968)
- [2] A. Bengtson, D. Jones, R. Payling
Glow Discharge Optical Emission Spectrometry. John Wiley & Sons, Baffins Lane, Chichester, 1997.
- [3] I. M. Dharmadasa, M. Ives, J. S. Brooks and Ch. Breen
Glow Discharge Optical Emission Spectrometry. John Wiley & Sons, Baffins Lane, Chichester, 1997.
- [4] Z. Weiss
Depth Analysis of Nickel Thin Films on Silicon by Glow Discharge Spectroscopy: the Interface Region. *Surface and Interface Analysis*, Vol. 15, 775-780 (1990).
- [5] K. Wetzig, S. Baunack, V. Hoffmann, S. Oswald, F. Präßler
Quantitative depth profiling of thin layers. *Fresenius J. Anal. Chem.* (1997) 358:25-31.
- [6] V. Hoffmann, H-J. Uhemann, F. Präßler, K. Wetzig and D. Birus
Fresenius J. Anal. Chem. (1997) 355:826.
- [7] F. Präßler, V. Hoffmann, J. Schumann and K. Wetzig
Comparison of Depth Resolution for Direct Current and Radiofrequency Modes in Glow Discharge Optical Emission Spectrometry. *Journal of Analytical Atomic Spectrometry*. September 1995, Vol. 10, pp.677-880.
- [8] U. Beck, G. Reiners
Dielectric reference coatings for the evaluation of thin film characterisation techniques. *Thin Solid Films* 270 (1995) 85-90
- [9] U. Beck, G. Reiners, Th. Wirth, V. Hoffmann, F. Präßler
Multilayer reference coatings for depth profile standards. *Thin Solid Films* 290-291 (1996) 57-62
- [10] M. Winchester, U. Beck
Availability of Layered Certified Reference Materials for Industrial Application of Glow Discharge Spectrometric Depth Profiling. *Surface and Interface Analysis*, 27 (1999) 930-935
- [11] U. Beck, Th. Wirth
VAMAS project in TWA 2. "Evaluation of reference coatings for quantitative GD-OES depth profiling" (1997)
- [12] S. Hofmann.
Practical Surface-Analysis by Auger and X-Ray Photoelectron Spectroscopy: Depth Profiling. John Wiley & Son Ltd. 1983
- [13] F. Präßler, V. Hoffmann, J. Schumann and K. Wetzig
Quantitative depth profiling in glow discharge spectroscopies - A new deconvolution technique to separate effects of an uneven erosion crater shape. *Fresenius J. Anal. Chem.* (1996) 355:840-846.
- [14] Z. Weiss.
Quantitative evaluation of depth profiles analysed by glow discharge optical emission spectroscopy: analysis of diffusion processes. *Spectrochimica Acta*, Vol. 47B, No.7, pp.859-876, 1992.
- [15] EC-network on analytical glow discharge spectrometry
<http://www.homepages.unl.ac.uk/~rogersi/gdsnet/rf-exp.html>
- [16] Federal Institute for Materials Research and Testing (BAM)
Certified Reference Materials Catalogue 2001
<http://www.bam.de/crm/>

Appendix 1: List of Participants

- Hakkarainen, Rautaruuki Steel Laboratoriopalvelu, Raahe, Finland
- M. Köster, IFU Institut für Umformtechnik; Lüdenscheid, Germany
- Huan-Chien Tung, Lin Hai Industrial District, Taiwan
- O. Zywitzki, Institute für Elektronenstrahlphysik und Plasmatechnik, Dresden, Germany
- S. Trampert, Österreichisches Forschungszentrum Seibersdorf GmbH, Austria
- H. Jenett, ISAS Institut für Spektrochemie und Spektroskopie, Dortmund, Germany
- G. Heide, Technische Universität Clausthal, Germany
- O. Moreau, Shiva Technologies Europe, Ramonville Saint-Agne, France
- Z. Weiss, LECO Instrumente Plzen, Czech Republic
- M. Winchester, NIST National Institute of Standards and Technology, Gaithersburg, Maryland USA
- T. Asam, TAZ-GmbH, Seefeld, Germany
- V. Hoffmann, IFW Institut für Festkörperanalytik und Strukturforschung, Dresden, Germany
- Bengtson, SIMR Swedish Institute for Metals Research, Stockholm, Sweden
- J.-C. Hubinois, DTMN/AD/CA., France
- Th. Wirth, U. Beck, BAM Bundesanstalt für Materialforschung und -prüfung, Berlin, Germany
- K. Wagatsuma, IMR Institute for Materials Research Tohoku University, Tokyo, Japan

(Notice: Sequence of participants according to appendix 1 is different from numbering sequence according to appendix 3)

Attachment 1

Check list: Mailing

- a) the samples
- b) the analyzing conditions (according to attachment 2)
- c) the raw data (intensity vs. time linear scale) of the 3 identical measurements with optimized conditions both on paper and on disk (3 plots and 1 disks, labeled with your lab.-no)
- d) analyze the following elements for each depth profile
 - type A:** Si, Ti, B, Na, Ar, C, N, O, H
 - type B:** Ti, Al, Fe, Cr, Ar, C, N, O, H
- e) identify the spectral lines you have used for analysis
- f) comment on and identify problems you met during analysis (sample-, equipment-, discharge- and software-related)
- g) comment on the layer design and material selection of Round-Robin samples
- h) general comments

Appendix 2: Questionnaire of Project

Your lab-no. is:

dead line 1999-11-30

Attachment 2

Check list: Experimental conditions

1 Experimental set-up

1.1. Equipment

supplier:

polychromator: type:

monochromator: type:

other: type:

1.2. System configuration:

dc-mode:

rf-mode: matching type: free running type:

rf/dc-mode: matching type: free running type:

rf-front coupling: rf-back coupling:

GD-source: mm

GDS-pump: oil free? Yes: No:

spectrometer pump: oil free? Yes: No:

sample cooling? Yes: No:

GDS-cooling? Yes: No:

base pressure: Pascal

Ar purge time: sec.

2 Analytical parameters

2.1. dc-mode

parameters hold constant:

const. voltage: $U = \square\square\square\square$ V

const. current: $I = \square\square$ mA

const. flow: $F = \square\square\square$ sccm

const. pressure: $p = \square\square\square\square$ Pascal

parameters under control:

regulated voltage: $U = \square\square\square\square$ V

regulated current: $I = \square\square$ mA

regulated flow: $F = \square\square\square$ sccm

regulated pressure: $p = \square\square\square\square$ Pascal

2.2. rf-mode

Ar-flow: $F = \square\square\square$ sccm

Ar pressure: $p = \square\square\square\square$ Pascal

parameters under control:

a) measured in the rf-generator:

free running type:

U_{pp} : $U_{pp} = \square\square\square\square$ V

U_{dc} : $U_{dc} = \square\square\square\square$ V

I_{dc} : $I_{dc} = \square\square\square\square$ mA

Appendix 2:

Questionnaire of Project

matching type:

$P_{\text{forward}} =$

$P_{\text{reflected}} =$

b) measured at the sample:

U_{rf} : $U_{\text{rf}} =$ V

I_{rf} : $I_{\text{rf}} =$ mA

P_{rf} : $P_{\text{rf}} =$ W

U_{bias} : $U_{\text{bias}} =$ V

3 Software

3.1. Equipment software

supplier:

version:

home made:

3.2. Data format if different from ASCII:

4 Spectral lines:

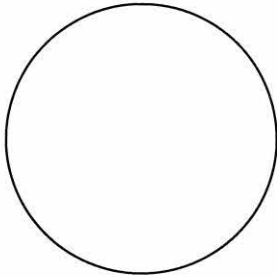
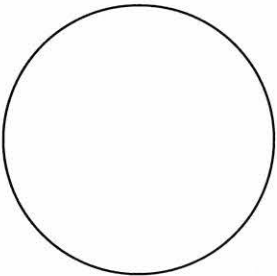
sample type A:

Element	Ti	Al	Fe	Cr	Ar	C	N	O	H
line[nm]									

sample type B:

Element	Si	Ti	B	Na	Ar	C	N	O	H
line[nm]									

5 Measurement craters - depth profiles:

sample	depth profile plot /data file
type A 	
type B 	

Appendix 3: Sample - laboratory matrix (anonymous)

lab #	Ti/Al on 100Cr6 steel	TiO ₂ / SiO ₂ on BK7-glass
2	159-453	-
3	159-484	123591-23
11	158-532	-
12	159-342	123591-29
13	159-345	123591-30
14	158-339	-
18	159-352	123591-31
20	158-531	-
25	158-481	-
26	158-433	-
28	158-524	123591-11
29	158-468	-
30	159-365	123591-009
31	159-349	-
34	158-421	123591-005
36	158-423	123591-004

Appendix 4: Profilometry: crater volume and area

Table 24: Profilometry: crater volume and crater area for Ti/Al on 100Cr6 steel

lab #	standard conditions					
	crater designation	crater classification	total crater area A [mm ²]	rim area [%]	total crater volume V [mm ³]	rim volume [%]
2	6	i	17,9	10,3	0,04	8,1
3	B1	i	18,1	8,6	0,07	4,7
13	3 (rf)	i	6,3	11,0	0,02	3,0
	4 (dc)	i	6,2	11,7	0,02	2,5
18	cc	i	5,9	24,4	0,03	12,4
25	2	i	18,1	13,1	0,03	7,8
26	B	i	19,2	5,4	0,09	1,5
29	3	i	18,5	6,6	0,04	1,8
31	10	i	18,9	7,5	0,04	4,1
	12	i	18,3	7,5	0,04	4,7
36	02	iii	8,7	0,0	0,07	0,0

Table 25: Profilometry: crater volume and crater area for Ti/Al on 100Cr6 steel

lab #	optimised condition					
	crater designation	crater classification	total crater area A [mm ²]	rim area [%]	total crater volume V [mm ³]	rim volume [%]
2	1	i	19,6	17,0	0,07	24,9
3	B5	i	17,5	12,8	0,09	26,2
11	1 / 3	iii	18,8 / 18,8	0,0 / 0,0	0,06 / 0,06	0,0 / 0,0
13	5	i	6,3	5,9	0,02	0,8
14	2 (rf)	iii	-	-	-	-
18	ea	i	7,1	6,1	0,04	1,2
20	1	iii	-	-	-	-
25	6	i	18,1	12,1	0,05	8,8
28	1	iii	-	-	-	-
30	2	i	19,1	8,2	0,08	2,4
36	3 (dc) / 16(rf)	iii / ii	8,3 / 7,8	0,0 / 0,0	0,05 / 0,02	0,0 / 0,0

Appendix 4: Profilometry: crater volume and area

Table 26: Profilometry: crater volume and area for $\text{TiO}_2/\text{SiO}_2$ coatings on BK7 glass

lab #	optimised condition					
	crater designation	crater classification	total crater area A [mm ²]	rim area [%]	total crater volume V [mm ³]	rim volume [%]
13	1 5	i	5,7	30,6	0,01	13,1
			5,4	12,0	0,01	1,8
18	2	iii	12,3	0,0	0,03	0,0
34	10	ii	11,3	0,0	0,02	0,0
36	5	i	5,6	32,4	0,02	15,4

A Brief History of BAM

- 1870** The Prussian Ministry of Commerce, Trade and Public Works announces the establishment of a Mechanical and Technical Research Institute. Its task is to perform experiments of general scientific and public interest and to test the strength of components.
- 1904** The Royal Materials Testing Office is established in Berlin-Dahlem following the merger of the Royal Mechanical Testing Institute with the Royal Testing Station for Building Materials (founded in 1875) and the Royal Chemical Technical Testing Office (founded in 1877).
- 1919** Renamed the Public Materials Testing Office (MPA), the institute is responsible to the Prussian Ministry of Science, Fine Arts and Public Education; from 1936 the Public X-ray Investigation Office is included.
- 1920** The State Chemical Technical Institute (CTR) is established under the State Ministry of the Interior from the Military Testing Office, established in 1889 as the Central Research Office for Explosives.
- 1945** MPA and CTR are united and operate under the jurisdiction of Berlin City Council.
- 1954** The Federal Republic of Germany takes over responsibility for MPA/CTA as Federal Institute for Mechanical and Chemical Testing (BAM), renamed the Federal Institute for Materials Testing in 1956. In addition BAM takes over responsibility for public materials testing for the state of Berlin.
- 1969** Under the Statute on Explosive Substances BAM is granted the status of higher federal authority; an amendment to the law in 1986 adds the word "research" to BAM's title.
- 1975** Under the Statute on the Transport of Hazardous Goods BAM is given greater responsibility in the field of public technical safety.
- 1990** German reunification and a recommendation from the German Scientific Council strengthen BAM's function as a federal chemical technical institute. Its personnel is increased by staff gained from the defunct Office for Standardisation, Measurements and Product Testing (ASMW) and Academy of Sciences in the former GDR. Responsibility for public testing for Berlin is gradually ended.
- 1995** Following extensive reorganisation, under a decree from the Federal Ministry of Economics BAM is given a new statute, revised management structures and methods and a future-oriented profile as an essential element of the technical and scientific infrastructure of the Federal Republic of Germany.
- 1998** Under an amendment to the Statute on Explosive Substances, the European Directive on Explosives from 1993 is adopted into Federal German Law. It names BAM as the competent authority. Confirming BAM's position as higher authority, it links BAM as Notified Body to the European System of Conformity Assessment.
- 1999** Under the framework agreement between the Federal Institute of Physics and Metrology (PTB) and BAM covering metrology in analytical chemistry, BAM is included in the global cooperation of the Metre Convention and "Arrangement for mutual recognition of national standards and calibration certificates issued by national metrology institutes".

